Flow of temperate ice by grain boundary melt transport: theory vs experiments and implications for ice-sheet dynamics

B.G.A. van Oosterhout
Student number: 4070658

Supervisor: Prof. Dr. Chris J. Spiers
MSc Thesis
GEO4-1520
Credits: 30 ECTS

Utrecht University
Oktober 2019

Contents

Abstract

Ice sheet dynamics play a vital role in the Earth's climate and a key question is if melting of the ice sheets contributes to sea level rise. The dynamics of ice sheets are controlled by rheological behavior at the grain-scale. Rheological behavior can be described by a flow law of the form:

$$\dot{\epsilon} = A\frac{\sigma^n}{d^p}exp\Big(\frac{-Q}{RT}\Big) \tag{1}$$

in which n and p denote respectively the stress and grain size exponent. The rheology of ice at high stress (>1 MPa) is attributed to dislocation creep, with n=3 and p=0. At low stress (<0.1 MPa), there is evidence for a decrease in stress-exponent which has been attributed to grain boundary sliding (GBS) with n=1.8. It is assumed that the contribution of grain boundary processes, such as diffusion creep, which would be characterized by n=1, are insignificant in ice. However, ice creep experiments show a sharp increase in strain-rates of a factor of 5-10 close to the melting temperature (T_m). Optical reflectivity measurements and thermodynamic calculations indicate that above T$\sim$262 K liquid films are present on the surfaces and grain boundaries of ice. The thickness of these films increase in ice close to T_m, with a thickness of 2-5 nm at T=272 K. A fluid film of this size has nearly the same viscosity as bulk water. The question addressed in this thesis is if flow by grain boundary melt transport can contribute to the deformation of ice close to T_m and can account for the observed increase in strain-rates. This process is expected to be controlled by the slowest of three steps: (1) melting, (2) transport through the grain boundary and (3) freezing. Hence, it can be envisaged as an analogue of pressure solution creep in rocks.

In this thesis, pressure solution theory is modified to construct a grain-scale model for melt-assisted creep in polycrystalline ice. This model is modified to explain the behavior of a wire cutting through ice, since it is expected that this process is controlled by the same kinetics. An attempt is made to perform wire regalation experiments to verify these models and to test if experiments show the same stress and wire diameter/grain-size exponent. This theory predicts that melt-assisted creep in polycrystalline ice is controlled by the transport-step, as melting and freezing rates are 3 orders of magnitude faster. The mechanism can be described by n=1 and p=3. At low stress ($\leq$0.1 MPa) and small grain size (1 mm), the polycrystalline model predicts a transition to melt-assisted creep at T$\sim$272.6 K. A stress-exponent of n=1 is observed in some creep experiments on polycrystalline ice close to T_m. Experimental data on the wire regalation velocity confirms the dependency on wire diameter, but there is no conclusive creep data close to the melting temperature to contradict or confirm the grain-size exponent in polycrystalline ice.

Melt-assisted creep may play a role in the rheology at the base of ice sheets, where the temperature is close to T_m. However, there is substantial ice core data that show an increase in grain size close the base of the ice sheets. This suggest that grain growth by migration recrystallization is occurring, which does not favor grain size sensitive (GSS) creep. In some layers of the ice sheet, the presence of impurities inhibits grain growth and melt-assisted creep may be the dominant deformation mechanism. Conventional flow laws for ice rheology do not consider this effect and may underestimate strain-rates in these layers. However, in these layers a strong CPO is observed and it remains questionable whether this can be reconciled with flow by grain boundary melt transport as dominant deformation mechanism.

1 Introduction

1.1 General background

Glaciers and ice sheets cover 9.6% of the surface of present-day Earth and during the last glacial maximum (LGM), 21 kyr ago, ca. 22% of the Earth's surface was covered with ice sheets. At present-day most of the ice is locked up in the polar ice sheets of Antarctica (25.7×10^6 km^3) and Greenland (2.85×10^6 km^3) (Marshall 2005), equivalent to respectively 61.1 msl and 7.2 msl (meters of global sea level rise). A small volume fraction of ice (0.7%) is locked up in other polar areas and mountain ranges, but these glaciers play an important role in fresh water supply in many regions.

An important topic in the current debate on global change is how climate change will affect future sea level rise. A key question is to what extent melting of the polar ice sheets contributes to sea level rise at present and in the future (Stocker et al. 2014). There are three main contributors to sea level rise: (1) thermal expansion of the oceans (Church et al. 1991), (2) melting of sea ice and non-polar glaciers (e.g. Rothrock et al. 1999; Stroeve et al. 2007) and (3) melting of the Antarctic and Greenland ice sheets (Stocker et al. 2014). During the twentieth century the first two processes have been the dominant contributors to sea-level rise, but it is expected that the contribution of the third process will increase in the longer term and become more important in the decades, centuries and millenia ahead. The fifth IPCC report (Stocker et al. 2014) shows that the contribution of these ice sheets has increased over the past decades. The average rate of mass loss from the Greenland ice sheet has very likely increased from 34 Gt/yr (1992-2001) to 215 Gt/yr (2002-2011) (Ewert et al. 2012; Sasgen et al. 2012). The average rate of mass loss from the Antarctic ice sheet, mainly from the Northern Antarctic peninsula and the Amundsun Sea region, has likely increased from 30 Gt/yr (1992-2001) to 147 Gt/yr (2002-2011) (Thomas et al. 2011; Ivins et al. 2013). The expected contribution of melting of the polar ice sheets to sea level rise remains a key uncertainty in projections of climate change.

Crucial to the long term survival of ice sheets is the mass balance between accumulation and ablation (Rignot et al. 2011) (see Figure 1) and a rise in global atmospheric temperature does not necessarily causes an increase in melting rate of the ice sheets. Accumulation takes place by precipitation and ablation of the ice sheet takes place by: (1) calving of ice sheets into the ocean, (2) release of meltwater by runoff, (3) sublimation and (4) wind erosion (Alley et al. 2005; Bintanja and Van de Wal 2008). The melting of ice and calving of icebergs is limited to the edge of the ice sheet where the ice sheet meets the ocean. Sublimation and wind erosion play a role on the interior of the ice sheets but these two processes are quantitatively negligible compared to melting at the edge of the ice sheets. Therefore, the transport (flow) rate of ice from the interior to the margin of the ice sheet determines how much ice there is available for melting. The observed flow velocities of the Greenland and Antarctic ice sheets are shown in Figure 2.

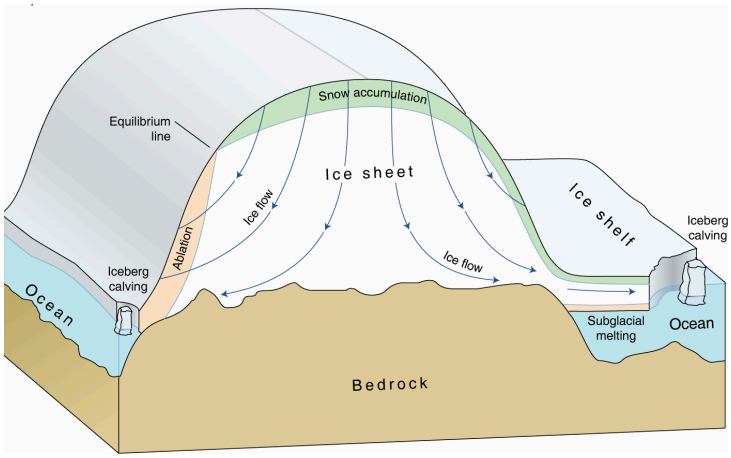

Figure 1: *Schematic representation of an ice sheet resting on the bedrock, with the accumulation (green) zone and ablation (orange) zones and the flow lines (blue) indicating ice flow. Left part of the ice sheet can be envisaged as an analogue of Greenland ice sheet situation, whereas the right part displays the ice shelf situation of the Antarctic ice sheet (picture taken from lima.nasa.gov/antarctica).*

The flow-rate of ice depends on two mechanisms: internal deformation of the ice sheet (e.g. Duval et al. 1983; Montagnat and Duval 2000; Goldsby and Kohlstedt 2001; Faria et al. 2014a) and sliding of ice over the bedrock (e.g. Krabbendam et al. 2016). Quantitative understanding of the dynamics of these ice sheets is thus of great importance for climate models as well as predictions on the response of ice sheets on climate change in the coming decades and centuries.

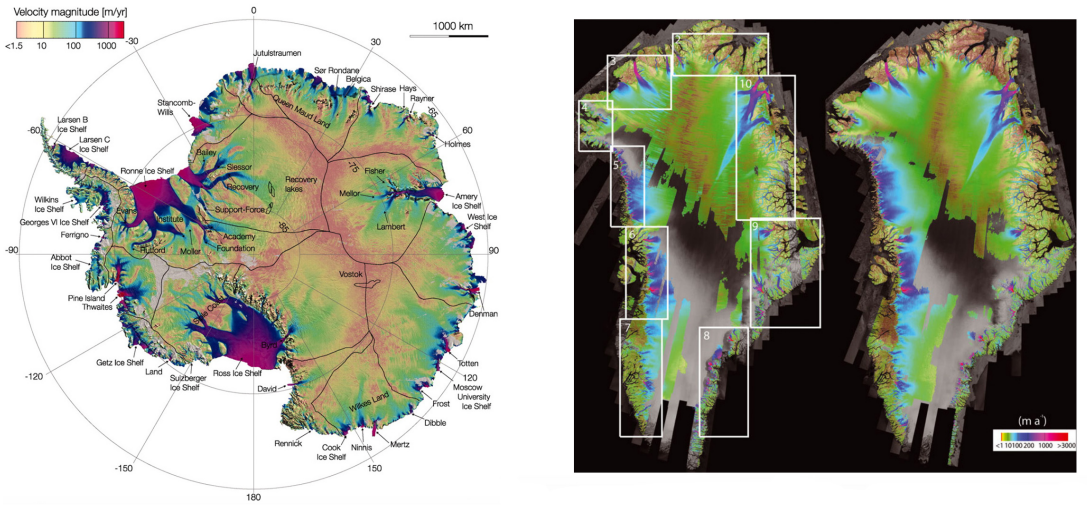

Figure 2: *(a) Antarctic ice sheet and shelf velocities based on satellite radar interferometry (after Rignot et al. (2011)). Black lines indicate major divides. (b) Flow velocities of Greenland ice sheet for the winters of 2000/01 (left) and 2005/06 (right), based on satellite radar interferometry (after Joughin et al. (2010)).*

1.2 Introduction to ice sheet dynamics and rheology

In order to understand the dynamics of ice sheets theoretical and numerical models have been conceived based on: (1) internal deformation of the ice (rheological behavior, e.g. Glen 1955; Schulson and Duval 2009a; Goldsby and Kohlstedt 2001); (2) interactions with the landscape (which includes both sliding of ice sheet over the bedrock as well as deformation of the bedrock itself) (e.g. Alley et al. 1986; Hindmarsh 1997; Cuffey and Paterson 2010); (3) the hydrological cycle (Marshall 2005) and (4) ocean-atmosphere-ice sheet system (e.g. Driesschaert et al. 2007). Previous research has been aimed at understanding the microphysical processes of ice under different boundary conditions like stress, temperature and deformation mode in order to derive rheological flow laws for the internal deformation of the ice (Steinemann 1954; Glen 1955; Duval et al. 1983; Goldsby and Kohlstedt 2001; Schulson and Duval 2009b), because the macroscopic internal behavior of ice sheets is for a large part controlled by microscopic physical processes at the grain-scale.

Significant progress has been made in the understanding of the rheological behavior of ice since the 1950's. Creep experiments performed at high stresses have been used to derive Glen's flow law (Glen 1955; Paterson 1994), which is the most commonly used flow law for modelling ice sheet dynamics. Glen's flow law can be viewed as based on the Weertman model for dislocation climb (Weertman 1955) and is given by:

$$\dot{\epsilon} = A\sigma^3 exp\Big(\frac{-Q}{RT}\Big) \tag{2}$$

in which A is the material parameter of ice and Q is the apparent activation energy. This flow law assumes that ice deforms by a single deformation mechanism, namely dislocation creep, in which stress is related to strain using a power-law with a stress exponent of n$\sim$3. At low stresses, the strain-rates are small ($<10^{-10}s^{-1}$) and it becomes difficult to obtain reliable data. However, there is a clear indication of a decrease in the stress-exponent and grain size sensitive (GSS) creep when stresses are lower than 0.1 MPa (Mellor and Testa 1969; Barnes and Tabor 1969; Colbeck and Evans 1973; Schulson and Duval 2009a; Goldsby and Kohlstedt 2001). Goldsby and Kohlstedt (1997, 2001) suggested that at low stresses the behavior of ice can be characterized by a stress-exponent of 1.8-2.4 and associated this low stress

regime to GSS grain boundary sliding (GBS) dominated creep, accommodated by basal slip. Montagnat and Duval (2000) and Duval and Montagnat (2002) associated deformation at lower stresses with basal slip accommodated by strain induced grain boundary migration (e.g. dynamic recrystallization).

In many polycrystalline materials, diffusion becomes important at low stresses/temperatures and small grain sizes (Duval 1977) and is also characterized by a low n-value (theoretically n=1). There have been attempts to find evidence for diffusion in very fine grained ice (e.g. Stern et al. 1997), but microstructural observations show that even at a grain size of 3-5 μm grain boundary diffusion (coble creep) is inaccessible even at low stresses (<0.1 MPa) and low temperatures ($\sim$ 200 K). There is however another regime at which grain boundary transport mechanisms may play a role in the deformation of ice. At temperatures close to the melting point, pressure melting or pre-melting accounts for the presence of liquid-like layers at the grain boundaries of ice (Dash et al. 2006) (see section 2.4.1 for thermodynamical background). The presence of such a liquid layer can increase the effect of grain boundary diffusion or, when of sufficient thickness, viscous flow in the grain boundary due to a pressure gradient. The principle is that ice melts at highly stressed grain boundaries or is present in equilibrium as pre-melted layer and the liquid is squeezed out and transported to lesser stressed grain boundaries where it refreezes, hence leading to strain (e.g. Krabbendam et al. 2016) (see Figure 3). The kinetics of this stress-driven melting and freezing creep are expected to be determined by the slowest step of melting, transport and freezing analogous to pressure solution creep in other polycrystalline or granular aggregates (e.g. Rutter 1976; Spiers and Schutjens 1990; Pluymakers and Spiers 2015). In this study, I refer to this sequence of grain boundary melting, freezing and transport processes as melt-assisted creep. However, the term melt-assisted creep is also used in a general sense to explain the observed increase in strain-rates close to the melting temperature of ice, regardless of the underlying mechanism(s). An increase in grain boundary sliding, enhanced dislocation creep and especially fast dynamic recrystallization may also be associated with the increase in fluid film thickness close to the melting temperature (Duval et al. 1983).

Noting its resemblance to pressure solution creep, it is expected that melt-assisted creep becomes more important when the grain size decreases and depending on whether the interface or transport kinetics are rate-determining an inverse dependence on grain size of p=1-3 is expected, as well as a stress-exponent of n=1. This mechanism may enhance creep rates in ice close to the melting temperature and if the kinetics of this mechanism are fast enough, then a switch from plastic deformation (basal slip accommodated by GBS and/or dislocation creep) to melt-assisted creep via the grain boundary may occur just below or at the melting temperature of ice (e.g. Morgan 1991; Krabbendam 2016).

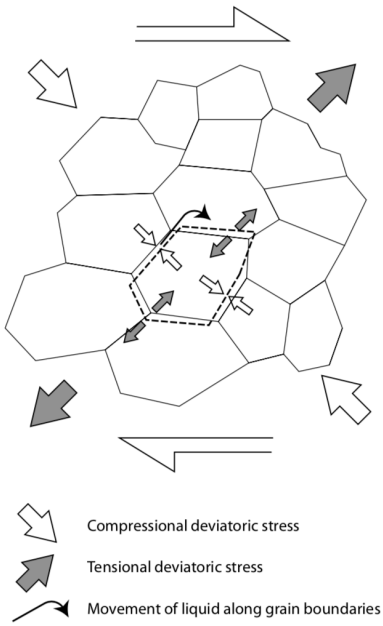

Figure 3: *Schematic drawing of melt-assisted creep by grain boundary transport. Melting occurs at highly stressed grain boundaries and refreezing at lesser stressed grain boundaries (After Krabbendam (2016)).*

It is still a topic of debate (e.g. Goldsby and Kohlstedt 2001; Duval and Montagnat 2002; Faria et al. 2014a) which deformation mechanisms are active in ice sheets under different boundary conditions such as temperature, grain size and stress and each deformation mechanism requires its own flow law. Solely making use of Glen's flow law to describe the flow in ice sheets over the complete range of boundary conditions has proven to be inaccurate (Goldsby and Kohlstedt 1997; Throstur Thorsteinsson et al. 1999). GSS creep at low stresses can be attributed to (grain boundary) diffusion, GBS and melt-assisted creep: all three are favored by a small grain size and liquid present at the grain boundaries.

To experimentally test the stress and grain-size exponent in ice close to the melting point requires production of very fine grained dense polycyrstalline ice (e.g Goldsby and Kohlstedt 1997). As grain size sensitive mechanism at low stresses can only be tested if the grain size is a few orders of magnitude smaller than natural occurring ice, as strain-rates should be readily measurable in the lab. This requires a very challenging technique of transforming natural occurring hexagonal ice (I_h) to the high-pressure ice II phase, followed by a rapid decrease in pressure and transformation back to I_h at T<200K (Stern et al. 1997). Therefore, wire regalation experiments were performed. In wire regalation experiments, a loaded wire slowly cuts through the ice by: (1) the formation of a liquid-layer in between the ice and the wire, (2) squeezing out the liquid layer around the wire and (3) refreezing at the top of the wire. Hence, it is expected to be controlled by the same kinetics as melt-assisted creep and the wire diameter can be used as an analogue for grain size.

1.3 Aims and scope of this thesis

The aim of this study is to predict strain-rates for melt-assisted creep by providing a theoretical model and by performing experiments on ice. In this thesis, I will present a review of the current knowledge on creep mechanisms in ice and I will modify pressure solution theory (e.g. Pluymakers and Spiers 2015) for melt-assisted creep in ice based on: (1) the driving force, (2) the kinetics controlling the rate of melting, freezing and transport and (3) the geometry and properties of ice crystals and their grain boundaries. This theoretical model can be used to develop an equation in which deformation is related to stress for melt-assisted creep and an attempt is made to test the characteristics of this mechanism with wire regalation experiments. The results of the model are extrapolated and compared with creep experiments on polycrystalline ice to assess the relevance of melt-assisted creep in ice sheet dynamics.

2 A review of ice rheology and deformation mechanisms

2.1 Properties of single ice crystals

Under natural pressure-temperature conditions on the Earth's surface, ice occurs in the ordinary hexagonal form (I_h, see Figure 4a). The melting temperature of ice is 273,15 K at atmospheric pressure, which implies that all of the ice at the Earth's surface is relatively close to its melting temperature. The hexagonal lattice is characterized by a low density compared with water, with an atomic packing factor of less than 34%. The water molecule in this lattice consists of one oxygen and two hydrogen atoms and each oxygen atom is surrounded by four other oxygen atoms by two covalent and two hydrogen bonds to form a tetrahedron. The tetrahedrons are organised in parallel (basal) planes (0001). The axis normal to this plane is the c-axis [0001]. Due to its symmetry there are three identical axes at an angle of 60°with the basal plane: the a-axes $<1\bar{2}10>$. The structure of the crystal lattice of ice and the orientation of planes is relevant for plastic deformation by movement of dislocations through the lattice. Dislocations are defects in the crystal lattice that form a distortion of the lattice. Without the presence of defects in the crystal lattice, plastic deformation would be much slower. There are two end-members of dislocations: edge and screw dislocations. Edge dislocations form an extra half plane in the crystal lattice. Screw dislocations are defects that cause the atoms to be arranged in a helical pattern normal to the direction of stress.

Table 1. Material properties of water

		Value	Unit
Melting temperature at 1 atm	Tm	273,15	K
Liquid density of water (at 0 °C)	ρw	999,8396	kg/m3
Solid density of ice (at 0 °C)	ρs	916,7	kg/m3
Molecular volume of liquid (at 0 °	Ωl	2,99E-29	m3
Molecular volume of solid (at 0 °(	Ωs	3,26E-29	m3
Liquid bulk viscosity (at 0 °C)	η(0,bulk)	0,001792	(N/m2) s

Under an applied stress, dislocations can move through the crystal lattice resulting in deformation of the crystal. The required stress to move dislocations through the lattice depends on the orientation of the crystal and the theory of dislocations forms the basis of dislocation creep in ice. Glide along the basal plane (0001) (see Figure 4b) is by far the easiest to activate (Duval et al. 1983). When a material experiences different creep rates in different crystallographic direction, it is called (plastic) anistropic. Its strong plastic anistropy makes it a good analogue for plasticity in anistropic rock-forming minerals, such as quartz and feldspar (e.g. Drury and Urai 1990). Melt-assisted creep is a grain boundary process (and thus intergranular) and does not rely on the plastic properties of the ice crystal. However, a full understanding of all the microphysical processes in ice is required to assess the relevance of melt-assisted creep. Deformation of polycrystalline solids in general takes place by the fastest parallel concurrent deformation mechanism under specific conditions (stress, grain size, temperature) and determining stress-strain relations requires a complete description of all the mechanisms involved.

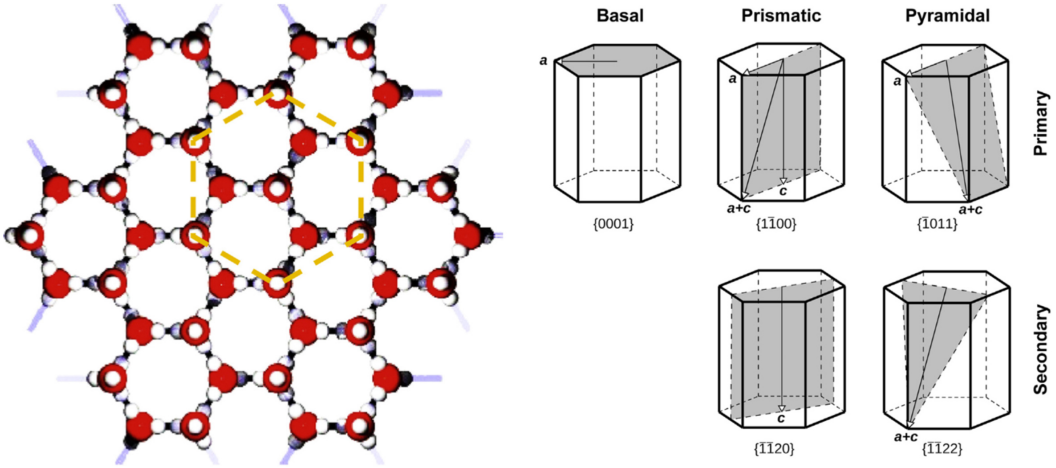

Figure 4: *(a) The crystalline lattice of ice I_h, after (Faria and Hutter 2001). Red spheres represent oxygen and white spheres represent hydrogen atoms. Perspective normal to basal plane. (b) Available slip systems in I_h, after (Hondoh 2000).*

2.2 The physical properties of glacial ice

Glacial ice is formed by compaction of precipitated snow. As new snow layers accumulate, the pressure increases in the underlying snow layers. Compaction takes place by sintering of the snow crystals and is accompanied by a decrease in porosity up to the point where the air pores are no longer connected and polycrystalline ice with isolated bubbles remains (Cuffey and Paterson 2010). At larger depths, the overburden pressure leads to shrinking of the air bubbles.

The temperature of ice in an ice sheet varies with depth and spatially. In the upper part of an ice sheet (excluding the first couple of meters), the temperature is identical to the annual average surface temperature, ranging from ~230 K in the central part of the Antarctic ice sheet (Rignot et al. 2011; Faria et al. 2014b) up to 273 K. At the base of an ice sheet, the geothermal heat flux and (locally) frictional heating generate heat and the temperature of the ice near the bedrock can reach the pressure-melting temperature (Faria et al. 2014b; Krabbendam 2016). The depth at which the temperature starts to increase depends on the amount of heat generated at the base. The rate of plastic deformation increases at higher temperatures (see section 2.3.1), as well as the thickness of liquid-like layers on the grain boundaries (see section 2.4.1). For an ice sheet it is useful to express the temperature in terms of difference with the pressure-melting temperature. At depth, the pressure results in a decrease of melting temperature and this will affect strain-rates. The pressure melting temperature can be calculated using:

$$T_{\mathrm{m}} = -C\Delta P \tag{3}$$

where T_m is the pressure-melting temperature (°C), C is the pressure melting constant of ice (9,8 10^{-8} °C Pa^{-1}, Lliboutry (1971)) and ΔP is the overburden pressure, which is given by:

$$\Delta P = \rho_{\mathrm{ice}} h_{\mathrm{ice}} g \tag{4}$$

where ρ_{ice} is the density of ice, g is the acceleration constant (ms^{-2}) and h_{ice} is the thickness (m). At the base of a typical ice sheet (e.g. at a depth of 2500m) this will result in a pressure-melting temperature (T_m) of -2.2°C (271K). The difference in temperature with the pressure melting point can be calculated using:

$$T^* = T - T_m \tag{5}$$

The grain size of ice in glaciers varies from less than a millimeter up to hundreds of millimeters and depends on impurity content, stress and strain (e.g. Cuffey and Paterson 2010). The upper part of an ice sheet is characterized by a gradual increase in grain area up to a few tens of mm^2 at a few hundred meters. In the lower part of the ice sheet grain size shows an inverse correlation with impurity content, but the mechanisms behind this are still unclear (Eichler et al. 2017). As temperature increases near the base of an ice sheet, the grain boundary becomes more mobile and grain area increases up to hundreds of mm^2 (Faria et al. 2014b). Besides variations as a function of depth there can be significant spatial variations in grain size as a result of variation in stress and impurity content. In general, the impurity content of ice deposited in interglacials is low, whereas the impurity content of glacial ice is relatively high. Deformation of ice at low stresses is sensitive to grain size (e.g. Goldsby and Kohlstedt 1997). Most theoretical treatments and laboratory experiments of grain boundary transport/diffusion processes (e.g. coble creep, pressure solution creep) also involve an inverse dependence on grain size (e.g. Rutter 1976; Pluymakers and Spiers 2015).

The stress in ice sheets is caused by its own weight and shape. The flow patterns in ice are very complex and are beyond the scope and scale of this study. In general, ice in the upper part shortens in the vertical directions and extends in the horizontal direction, whereas deep down the ice starts to deform by shear stress parallel to the surface slope. The shear stress can be approximated by local gravity-driven flow (Marshall 2005), which is given by:

$$\sigma_\tau = \rho_{ice} g (h_s - z) \frac{\delta h_s}{\delta x_i} \tag{6}$$

where z is the elevation (m), h_s (x,y) is the surface topography and i(x,y) refers to the horizontal plane and $\frac{\delta h_s}{\delta x_i}$ thus represents the surface slope of the ice sheet. This gives a reasonable approximation for the shear stress (Paterson 1994) that acts as a driving force and can be used for rheological flow laws in ice sheet modelling. The shear stress in ice sheets varies from less than 0.05 MPa at ice divides to 0.20-0.30 MPa in ice streams and outlet glaciers (Lüthi et al. 2002; Krabbendam 2016) (where the surface slope is large). Ice divides are the parts in the center of the ice sheets where the surface slope is small and flow velocities are low. Ice streams have a large surface slope and are the parts of the ice sheet that have the largest contribution to flow towards the oceans (see Figure 2). Figure 5 shows an example of how grain size and temperature vary with depth in the NEEM ice core of the Greenland ice sheet.

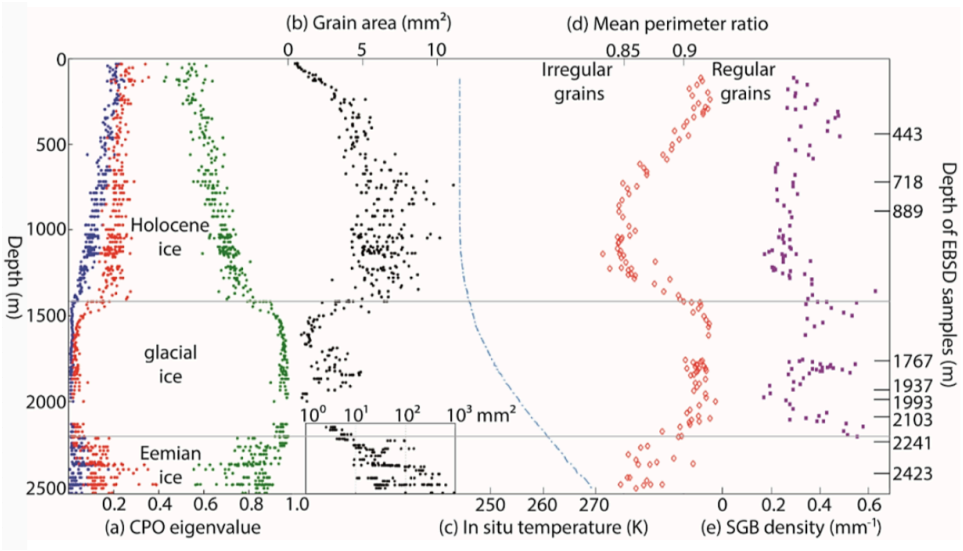

Figure 5: *Compilation of borehole data of the Greenland NEEM ice core (Eichler et al. 2013; Kuiper 2019), including (b) variations in mean grain area and (c) in-situ temperature.*

2.3 The creep of polycrystalline ice

The deformation behavior of polycrystalline ice at the centimeter to decimeter scale can be experimentally tested in the laboratory. Its mechanical behavior, as for any crystalline solid, can be generalized using rheological flow laws, in which deformation (strain or strain-rate) is related to an applied (differential) steady state stress. Rheological data for crystalline materials in general are presented using a power-law equation of the form:

$$\dot{\epsilon} = A\frac{\sigma^n}{d^p}exp\Big(\frac{-Q}{RT}\Big) \tag{7}$$

where $\dot{\epsilon}$ is the strain rate (ms^{-1}), A is a material parameter, σ is differential stress (MPa), d is grain size (m), n and p are respectively the stress and grain size exponent, Q is the apparent activation energy for the creep mechanism (J/K/mol), R is the gas constant (J/K/mol) and T is the absolute temperature (K). When modelling flow of natural ice the temperature requires a correction for the change in pressure-melting point (Equation **??**). The apparent activation energy Q reflects the amount of energy required for the reaction to occur. The study of creep in ice can be valuable for other minerals and crystalline materials (e.g. Drury and Urai 1990), because it is the only common mineral of which creep close to the melting temperature can be observed in nature and the laboratory on accessible timescales. In this section, an overview of different deformation mechanisms in ice is presented in the light of the present study and its characteristics (stress and grain size dependency) are discussed.

Under an applied stress, polycrystalline ice initially deforms viscoelastic. In nature this plays a role in tidal flexure in floating ice tongues on timescales from seconds to hours from the time of initial loading (Reeh et al. 2003). Initial viscoelastic deformation is not of any significance for studying ice sheet dynamics, since on timescales from days to millenia deformation of ice reaches a steady-state creep as it continuously deforms. In plastic deformation, this elastic response is followed by primary creep (see Figure 6 stage BC), in which deformation is taking place by the easy slip system (e.g. Schulson and Duval 2009a). This is followed by a decrease in strain-rate due to work hardening until a minimum strain-rate is reached (stage CD). The onset of dynamic recovery and recrystallization causes softening and the formation of a crystallographic preferred orientation (CPO). In this stage, the strain-rate accelerates due to enhanced basal slip up to the point where it reaches steady-state (stage EF). At this stage, the c-axes are aligned (see Figure 4) and no further softening can occur. Laboratory experiments hardly ever go beyond the minimum strain-rate, due to the long timescales involved.

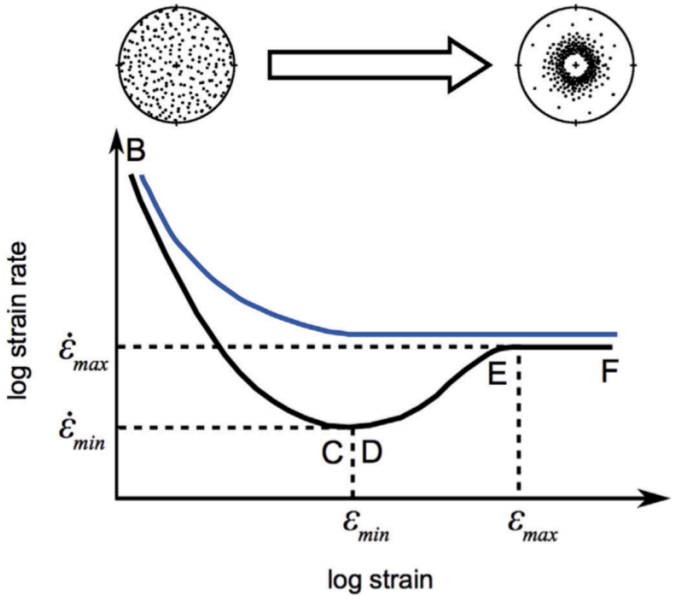

Figure 6: *Creep curve for initial anistropic ice (black) and initial isotropic ice (blue). The two plots on top show the formation of a lattice preferred orientation with increasing strain from initial anistropic ice. After Faria et al. (2014b) and Budd and Jacka (1989).*

2.3.1 Dislocation creep in ice and Glen's flow law

Uniaxial compression experiments on artificially isotropic polycrystalline ice at high stress (> 0.5MPa) were performed (Glen 1955; Steinemann 1954) to derive a power-law relation for ice rheology in the form of equation 1 to relate strain-rate to stress. Based on these experiments (see Table 2) a stress-exponent of n∼3 has been derived and Glen's flow law has been established, which is given as:

$$\dot{\epsilon} = A\sigma^3 exp\Big(\frac{-Q}{RT}\Big) \tag{8}$$

Glen's flow law assumes that creep is governed by a combination of basal and non-basal slip, in which the rate is limited by dislocation climb (Montagnat and Duval 2000; Schulson and Duval 2009a). A flow law for dislocation creep can be obtained by combining the theory of dislocation motion (Orowan's equation) and the theory for dislocation velocity based on the atomic jump model (e.g. Weertman model for dislocation climb, Weertman 1955). Dislocation motion is given by Orowan's equation as follows:

$$\dot{\epsilon} = \rho_{\mathrm{d}} b \bar{v} \tag{9}$$

where ρ_{d} is the density of mobile dislocations, b is the burgers vector and $\bar{v}$ is the average velocity of dislocations. The relation between dislocation density and stress is given by:

$$\rho_{\mathrm{d}} = \beta\sigma^2 \tag{10}$$

For dislocation climb, the glide velocity is controlled by the climb velocity at which dislocations of opposite sign annihilate and the average velocity between source and obstacle is given by:

$$\bar{v} = \frac{L}{d} v_{\mathrm{c}} \tag{11}$$

in which L is the distance between the two sources, d is the distance between two glide planes and v_c is the climb-velocity. The climb velocity in turn is controlled by the self diffusion, such that:

$$v_{\mathrm{c}} = \alpha\sigma D_{\mathrm{S}} \tag{12}$$

where α depends on the orientation of the slip plane with respect to the stress orientation and D_S is the self-diffusion coefficient, which in turn is given by:

$$D_{\mathrm{S}} = D_0 \exp\Big(\frac{-\Delta H_{\mathrm{S}}}{kT}\Big) \tag{13}$$

in which H_S is the activation enthalpy for self-diffusion. Combining equations 9, 10, 11, 12, and 13 results in:

$$\dot{\epsilon} = \alpha\beta b \frac{L}{d} \sigma^3 D_0 \exp\Big(\frac{-\Delta H_{\mathrm{S}}}{kT}\Big) \tag{14}$$

Generalization of equation 14 and combining the material parameters $(\alpha, \beta, b, L, d, D_0)$ leads to the generalised Glen's flow law (Equation 8). The above mathematical derivation leads to a stress exponent of n=3 and is thus in agreement with observed minimum strain-rates in laboratory experiments. It must be noted that creep accelerates after this minimum and on long-term dislocation creep in ice is more accurately described with a stress exponent of n=4. A lot of research has been conducted in constraining material parameter A to account for the effects of impurities (Jacka et al. 2003) and the role of ice fabric in promoting anistropic ice deformation (Throstur Thorsteinsson et al. 1999) and the creep activation energy (Q) has been established for different temperature ranges.

Table 2. Creep data for polycrystalline ice*	n	Q (kJ/mol)
	T < 263 K	
Glen (1955)	~3	
Steinemann (1958)	3.1-3.6	83
Mellor and Smith (1966)	3.5	45
Ramseier (1972)	3.1	59.9
	T > 263 K	
Glen (1955)	3.2	135
Steinemann (1958)	2.8-3.2	135
Mellor and Testa (1969a)	3.2	167
Barnes et al. (1971)	3.2	120

*All experiments were performed on grain size larger than 1 mm

2.3.2 Grain size sensitive creep at low stresses: GBS/SIBM + basal slip

Although dislocation creep in ice has been extensively studied under different boundary conditions, there is less knowledge about grain size sensitive (GSS) mechanisms in ice. This has two main reasons: (1) it is difficult to produce synthetic dense ice samples with grain sizes <1mm (at which GSS mechanisms become more important) (Stern et al. 1997) and (2) at a high (>1 MPa) stresses diffusion creep or other GSS mechanisms in ice are slow compared to dislocation creep. At low stresses (<0.1 MPa) there is significant evidence that shows a decrease in the stress-exponent (Barnes and Tabor 1969; Goldsby and Kohlstedt 1997). It is difficult to obtain convincing results in the laboratory, but there is agreement that its behavior can be described by a stress-exponent lower than n=2 (see Table 3) (Mellor and Testa 1969; Duval 1977; Goldsby and Kohlstedt 1997; Duval and Montagnat 2002). Observing GSS creep at accessible strain-rates in the laboratory ($>10^{-8}s^{-1}$) requires very small grain sizes in the range of 3 to 90 μm (e.g. Goldsby and Kohlstedt 1997), which can then be extrapolated to larger grain sizes. Possible grain size sensitive creep mechanisms are: (1) grain boundary sliding (GBS) + basal slip (Goldsby and Kohlstedt 1997, 2001), (2) strain induced grain boundary migration (SIBM) accommodating basal slip (Montagnat and Duval 2000; Duval and Montagnat 2002), (3) diffusion creep (Ashby and Verrall 1973) and (4) melt-assisted creep (Krabbendam et al. 2016).

Table 3. Low stress creep data for polycrystalline ice *	d (mm)	n	p	Q (kJ/mol)	T (K)
Steinemann (1954)	0.5-5	1.85			268
Glen (1955)		~1.5			260-273
Jellinek and Brill (1956)	1-2	~1		67	258-268
Butkovitch and Landauer (1960)	3-20	0.86-1.15		60	254-272
Mellor and Smith (1966)	0.8	~1		75	238-273
Bromer and Kingery (1968)	1-10	~1	1.95	50	260-270
Colbeck and Evans (1973)	2	1.3			273
Baker (1978)	0.6-1	2.8, 3.7	2.35		~265
Pimienta and Duval (1987)	1-2	~1.5			258
Duval and Castelnau (1995)	1	1.8			260

*All of the data was aquired over a stress range of 0.01 to 1 MPa

Goldsby and Kohlstedt (1997, 2001) performed compressive experiments with a constant stress at atmospheric pressure. At 236 K experiments on fine-grained ice (<100μm), deformation can be described by a stress-exponent of n=4 above $\sim$ 3-5 MPa, below occurs a transition to a stress-regime with n=1.8 and another stress regime change to n=2.4 is observed at a stress below $\sim$ 1 MPa (see Figure 7a). At temperatures above 258 K and grain-size data extrapolated to larger grain sizes, the transition to a stress-exponent of n=1.8 occurs below 0.5 MPa and a transition to the n=2.4 regime occurs only at a very low stress (10^{-3} MPa) and can be neglected (see Figure 7b). The n=1.8 regime can be described by a grain size exponent of p=1.4. Goldsby and Kohlstedt (2001) suggest that the mechanisms behind this grain size sensitive creep are basal slip and GBS. These two processes are sequential and act together, in which the slowest process determines the rate. Hence, at low stress basal slip controls the strain-rate (n=2.4) and at high stress GBS is rate-limiting (n=1.8). The mechanical data are in agreement with models of GBS accommodated by dislocation motion, which usually predict n=2 and p=2 (e.g. Ashby and Verrall 1973; Langdon 1994). This is substantiated by microstructural observations on samples deformed at low stress, that show now significant change in grain shape even at large strains, which

is expected in the diffusion and dislocation creep regimes (Padmanabhan and Davies 1980). Based on their results Goldsby and Kohlstedt (1997, 2001) introduced a composite flow law for ice rheology, which includes dislocation creep, diffusion creep and GBS/basal slip, which is formulated as follows:

$$\dot{\epsilon} = \dot{\epsilon_{\text{disl}}} + \dot{\epsilon_{\text{diff}}} + \Big(\frac{1}{\dot{\epsilon_{\text{basal}}}} + \frac{1}{\dot{\epsilon_{\text{GBS}}}}\Big)^{-1} \tag{15}$$

Under stress, grain size and temperature conditions in natural ice sheets, diffusion creep and basal slip limited GBS are very slow and the composite flow law becomes:

$$\dot{\epsilon} = \dot{\epsilon_{\text{disl}}} + \dot{\epsilon_{\text{GBS}}} \tag{16}$$

Both mechanisms can be expressed in the general form of equation 1 and the composite flow law can be written as:

$$\dot{\epsilon} = A_{\text{disl}}\sigma^{n_{\text{disl}}} * exp\Big(\frac{-Q_{\text{disl}}}{RT}\Big) + A_{\text{GBS}}\sigma^{n_{\text{GBS}}} * exp\Big(\frac{-Q_{\text{GBS}}}{RT}\Big) \tag{17}$$

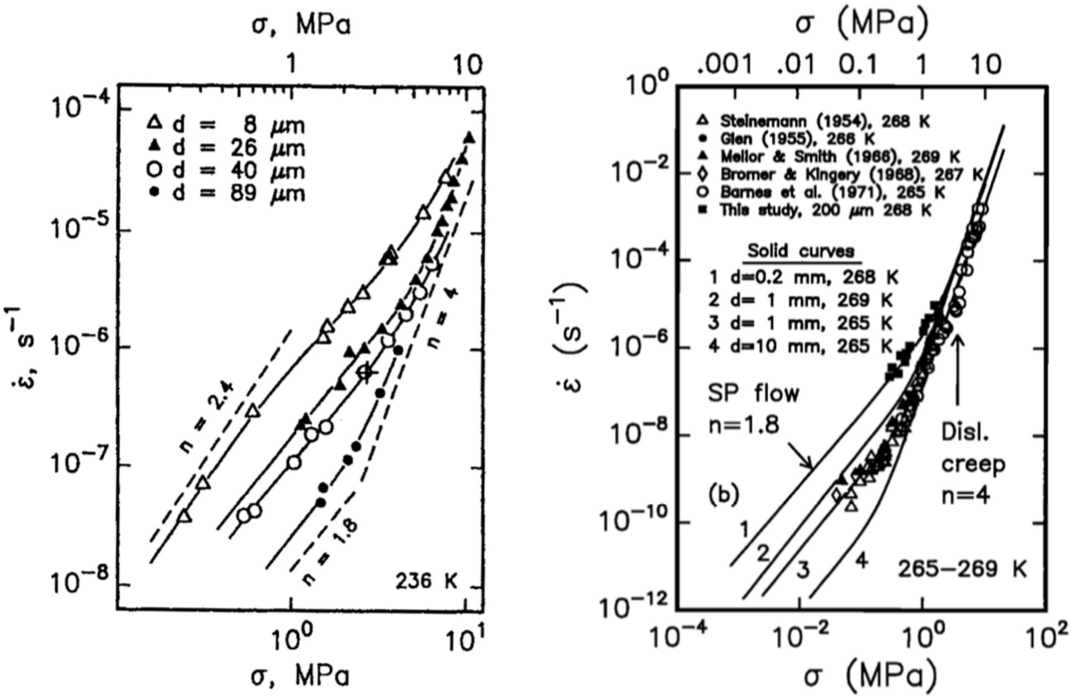

Figure 7: *(a) Creep experiments on fine-grained ice at 236 K (Goldsby and Kohlstedt 1997, 2001) showing transition from GBS/basal slip at low stresses (n=1,8/2.4) to dislocation creep (n=4) at high stresses and (b) compilation of creep experiments at 265-269 K (laboratory data extrapolated to larger grain sizes).*

However, GBS is generally believed to not be associated with the formation of a CPO (e.g. as shown in metals, Pérez-Prado et al. 1998) and numerical modelling from Zhang et al. (1994) shows that GBS weakens fabric development and result in an absence of a preferred orientation of the c-axes, in contradictions to observations in ice sheets (See Figure 5). Therefore, Duval and Montagnat (2002) suggest that it is more likely that strain induced grain boundary migration (SIBM) is the accommodating mechanism of basal slip in ice sheets. SIBM in turn is associated with migration recrystallization (Montagnat and Duval 2000; Duval and Montagnat 2002; Schulson and Duval 2009a). The driving force of this mechanism is the reduction in lattice energy stored in point defects: a grain boundary between a grain with a low and a high dislocation density tends to migrate into the grain with the higher dislocation density.

2.3.3 Diffusion creep

Diffusion creep is another possible mechanism for the deformation of polycrystalline materials that becomes increasingly important at low stresses and temperatures (e.g. Ashby and Verrall 1973). If a

crystal is subjected to a non-hydrostatic stress, then there is difference in free energy between grain boundaries with a high and a low normal stress. This generates a higher equilibrium concentration of vacancies at the stressed surface, generating diffusion of vacancies from the low to high stressed surface and diffusion of atoms in the opposite way. A smaller grain size results in a shorter pathway for diffusion making diffusion favorable in fine grained polycrystalline aggregates. Diffusion is characterised by n=1,p=2 for volume diffusion (Nabarro-Harring creep) or n=1,p=3 for grain boundary diffusion (Coble creep). A combined flow law for grain boundary and volume diffusion can be written as (Goldsby and Kohlstedt 2001):

$$\dot{\epsilon} = \frac{42\sigma V_\mathrm{s}}{kTd^2}\Big(D_\mathrm{v} + \frac{\pi\delta}{d}D_\mathrm{gb}\Big) \tag{18}$$

In which V_s is the molecular volume of the solid, D_v and D_{gb} are respectively the volume and grain boundary diffusion coefficients and δ is the grain boundary width. The diffusion coefficients are each of the form $D=D_0\exp(\frac{-Q}{RT})$. Diffusion creep is characterized by a linear stress/strain-rate relation with a stress exponent of n=1. The term σV_m represents the chemical potential which is the driving force of diffusion. Even for the smallest grain sizes (3-5 μm) at low stresses (0.1 MPa) and a temperature of 200 K (e.g. Goldsby and Kohlstedt 1997; Stern et al. 1997) no transition to an n=1 creep regime is observed Goldsby and Kohlstedt (2001) suggest that a transition to diffusion will take place at even lower stresses (see Figure 8), but this will occur at strain-rates that are too small to readily measure.

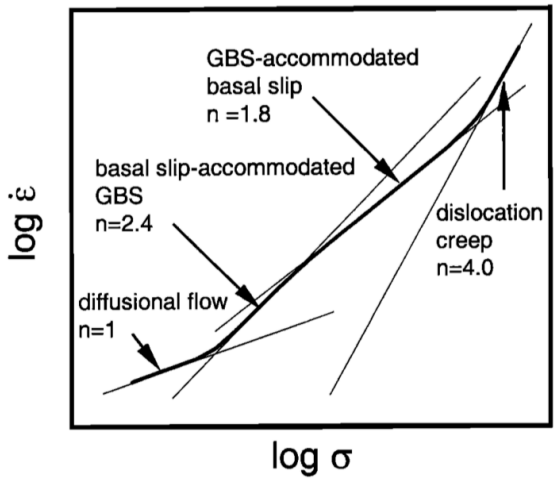

Figure 8: *Schematic diagram of the relative contributions of GSS mechanisms (diffusion,GBS/basal slip) and dislocation creep in ice as a function of stress. Figure taken from Goldsby and Kohlstedt (2001).*

However, Colbeck and Evans (1973) suggest a lower stress-exponent of n=1.3 at a constant temperature of 273,14 K and a stress of 0.01-0.1 MPa and Byers et al. (2012) concluded that ice flow around an obstacle in temperate ice (ice close to the melting temperature) behaves near linearly with a stress exponent of n<1.5. Linear Newtonian behavior (n=1) has been suggested for deformation mechanisms in thin ice sheets where shear stresses are low (Peltier 1998) and used for reconstruction of the North American Ice Sheet during the LGM (e.g. Marshall et al. 2002). The n∼1 behavior observed in some of these experiments in temperate ice suggest that there is a switch to Newtonian viscous flow. If grain boundary diffusion is not able to account for the observed near-linear behavior, then a solution may be provided in melt-assisted creep in which not grain boundary diffusion, but viscous flow is taking place (Barnes and Tabor 1969; Krabbendam et al. 2016).

2.4 Melt-assisted creep

Melt-assisted creep may play a role in ice close to the melting temperature (Morgan 1991; Schulson and Duval 2009a; Krabbendam et al. 2016) and could explain the increase in strain-rates observed close to the melting temperature (see Figure 9). This mechanism relies on the presence of liquid or liquid-like layers at the grain boundaries of ice (Dash et al. 2006). In a similar way as grain boundary diffusion, melt-assisted creep takes place by transport of matter from a highly to a lesser stressed surface in polycrystalline ice. The difference being that transport is possibly taking place by pressure-driven

viscous flow instead of grain boundary diffusion. The kinetics are likely to be governed by the slowest of the three serial processes: the melting of the highly stressed grain boundary, transport through the grain boundary or refreezing at the lesser stressed grain boundary. The mechanism of melt-assisted creep depends on: (1) the kinetics and thermodynamics of grain boundary pressure- and pre-melting, (2) the thickness and structure and flow properties of the fluid film as a function of temperature and (3) the pressure gradient in the grain boundary fluid as a function of externally applied stress. This can be used to predict under which conditions melt-assisted creep theoretically may play a role, or perhaps even become dominant, in polycrystalline ice and if these conditions occur in natural ice in ice sheets.

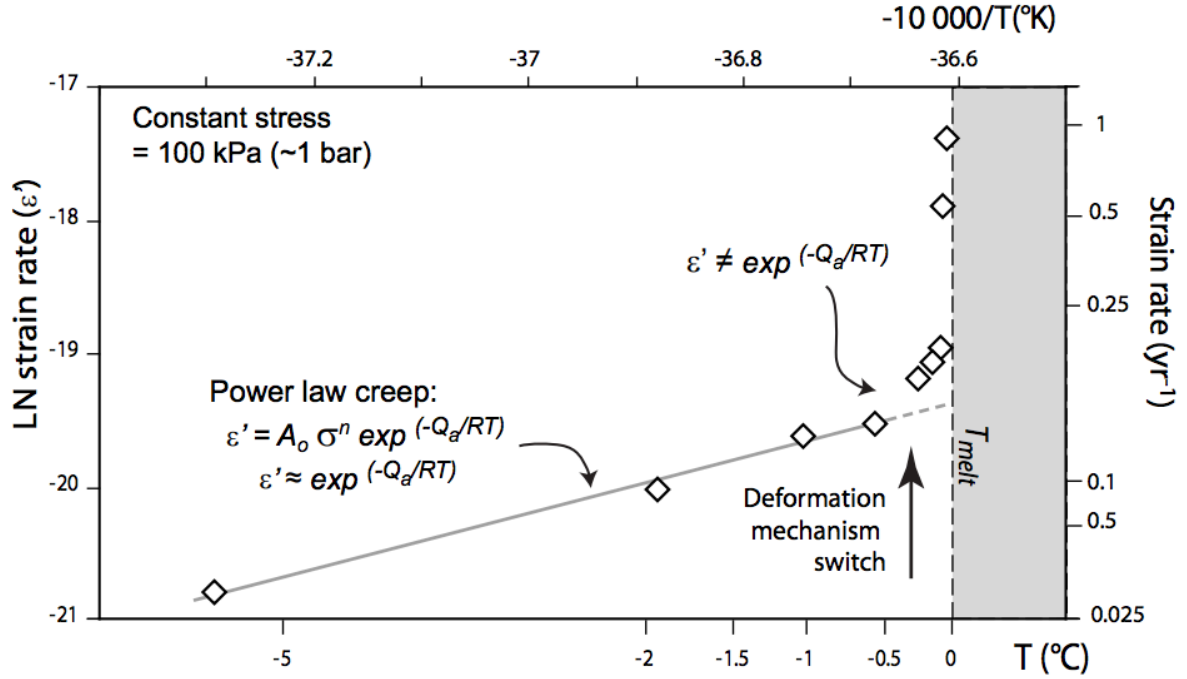

Figure 9: *Strain-rate against temperature at 0.1 MPa. After Morgan (1991) and Krabbendam et al. (2016).*

2.4.1 Pressure melting, pre-melting and flow properties of thin water films

The presence of a liquid layer on the surface and interfaces of ice has been known since the mid-nineteenth century when Michael Faraday observed the welding of two blocks of ice when the contact pressure was removed (Faraday 1850). Two explanations have been given for this phenomenon: (1) pressure melting and (2) surface or interfacial pre-melting. Pressure melting will occur because of a low density of ice with respect to water, which implies that ice melts under elevated pressures even at temperatures below the freezing point of water (Thomson 1861). This is essentially represented by the negative Clausius-Clapeyron slope between the ice and water phase in a P-T diagram and this mechanism has also been used as an explanation why ice is slippery; the pressure applied by the ice skate melts the ice below it and the water film acts as a lubricant (Joly 1887). However, the pressure required for pressure melting is $\Delta T_{\mathrm{m}} = 13.5$ MPa/K, which for ice at 266 K (that is observed to be slippery) would require 1000 kg/cm^2, suggesting there must be a different explanation for liquid water present at lower temperatures. Pre-melting can occur at temperatures as low as 258 K (Dash et al. 2006) and is based on lowering of the surface energy of ice (e.g. Kuroda and Lacmann 1982). Hence, it is favorable to have a thin film of water on an ice surface to lower the energy of the system. This explains why a liquid-like layer is present at equilibrium, several degrees below the melting point: (1) between a solid and its gaseous phase (Lifshitz theory), (2) due to interfacial melting in contact with a foreign solid (Fletcher 1973) and (3) due to grain-boundary melting in between ice crystals (Nye and Frank 1973). Interfacial melting with a foreign solid may very well take place at the base of ice sheets where the ice is in contact with the bedrock and grain-boundary melting may occur at the grain boundaries in polycrystalline glacial ice under the circumstances that the temperature is close to the melting point.

Liquid water therefore is likely to exist on grain boundaries if the temperature of the ice sheet is above 258 K. The effect of liquid water becomes more important when the temperature approaches the melting temperature and the thickness of the water film increases. The presence of liquid like layers can account for increased strain-rates as a result of: (1) enhanced grain boundary sliding (e.g. Goldsby and Kohlstedt 2001), (2) an increase in dynamic recrystallization (e.g. Duval and Montagnat 2002), which promotes crystal growth with a preferred orientation thereby enhancing easy basal slip, (3) viscous flow in the grain boundaries (e.g. Barnes and Tabor 1969) and (4) enhanced grain boundary diffusion (e.g. Goldsby and Kohlstedt 2001). Whether water transport through the grain boundaries is taking place by diffusion or viscous flow depends on the mobility of the liquid-layer. The mobility of the liquid layer in turn depends on its thickness and its structure, in particular if the molecules are "mobile" and able to flow. Thermodynamic calculations by Fletcher (1968) based on lowering the free energy of the molecular system, show that the thickness of the pre-melted liquid-layer exist above 243 K and the thickness strongly increases as the melting point approached, it can be approximated by:

$$w = C - 2,5log(-T) \tag{19}$$

where C is a constant between 2 and 5 nm and T is the temperature in degrees Celsius. At 272 K the thickness of the liquid layer is approximately 2-5 nm. Gilpin (1979) used wire regalation experiments and inferred that, assuming hydrodynamic flow, the fluid film thickness can be described using:

$$w = 3,5(-T)^{1/2.4} \tag{20}$$

in which T is the temperature in °C en w is the fluid film thickness in nanometers (see Figure 10). Measurements on the viscosity of water in thin films by Israelachvili (1986) show that the viscosity of films at the nanometer scale is still in the same order of magnitude as the bulk viscosity of water. A 10% increase in apparent viscosity is observed in films of about 5 nm. Chan and Horn (1985) show that only 1-2 molecular layers are immobilized at the surface and show that the effective viscosity of thin films with non-polar fluid can be calculated using:

$$\eta_{\text{eff}} = \frac{w}{w - 2W_{\text{s}}} * \eta_{\text{bulk}}(T) \tag{21}$$

in which W_s is the immobile region adjacent to a smooth surface and $\eta_{\text{bulk}}(T)$ is the temperature dependent viscosity of bulk water, which in turn is given by:

$$\eta_{\text{bulk}} = \left(1 + 0.0361(-T) + 0.0083(-T)^2\right) \tag{22}$$

in which T is the temperature in °C. Chan and Horn (1985) found that in non-polar fluids the thickness of W_s is in the order of 0,5-1,0 nm for tetradecane and hexadecane, which is in the order of only 1-2 molecular layers. Using the same approach for liquid water an immobile layer of 0,275 nm (size of one H_2O-molecule) up to 0,86 nm (two H_2O-molecules and the length of an hydrogen bond) can be expected, assuming that there is no additional effect of the H-bonds. For a liquid water film thickness of 5 nm this will result in approximately 12%-50% increase in viscosity for respectively 1-2 layers of H_2O-molecules. Pressure-driven viscous flow therefore seems to be possible down to a few degrees below 273 K, if the viscosity is corrected for the effect of immobilized layers. When the film thickness approaches 2-4 molecular layers the fluid film becomes immobilized and the fluid film can no longer be squeezed out and transport through the grain boundary can only take place by diffusion. If the ice is at the pressure melting point (273,15 K at 1 atm) stress on the grain boundary can increase the amount of water present at the grain boundary and active melting of the grain boundary takes place, instead of passive equilibrium melting. Figure 11 shows how the viscosity changes with temperature for 0-2 immobile layers by combining the equations for fluid film thickness (Equation 20) and viscosity (Equation 21 & 22).

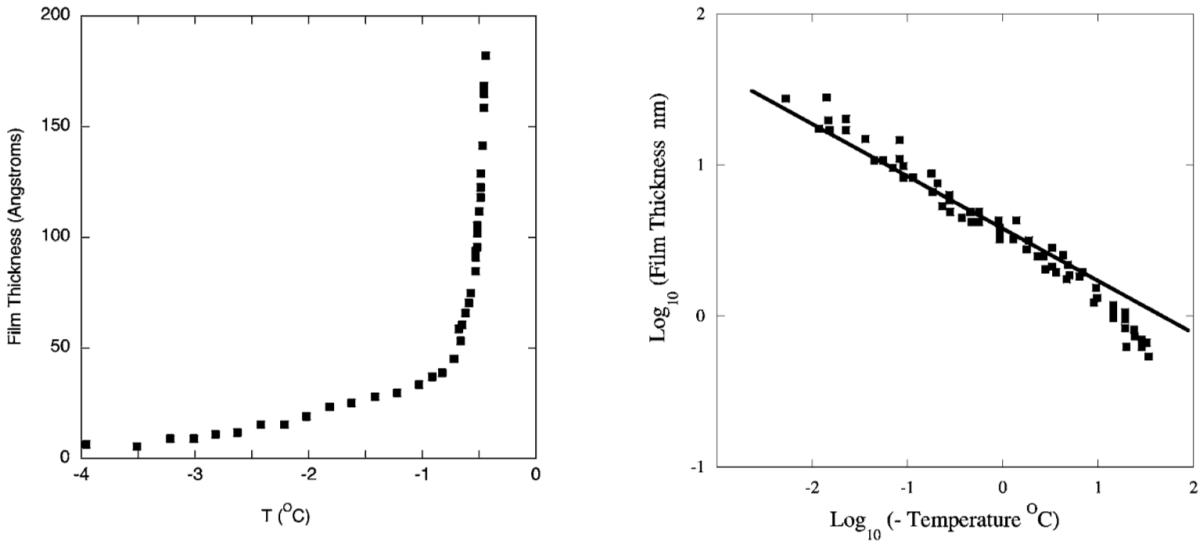

Figure 10: *(a) Optical reflectivity measurements of surface melting of ice in contact with air (after Elbaum and Schick (1991)). (b) Apparent thickness of water films inferred from wire regalation experiments by Gilpin (1980).*

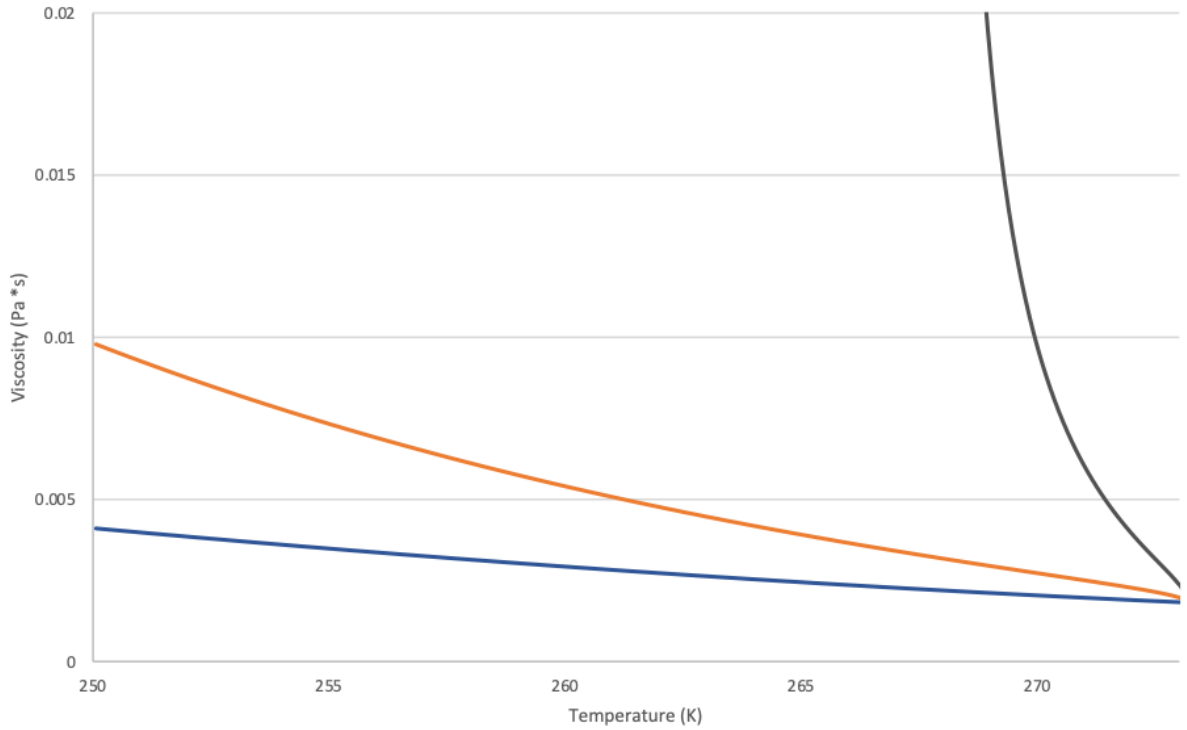

Figure 11: *Viscosity of the fluid film in the range of temperatures where the effects of pre-melting are expected to play a role based on Equations 20, 21 & 22. In the scenario of a 2 molecule thick immobile layer on each side of the grain boundary, viscous flow becomes very slow below 269 K.*

2.4.2 Theoretical basis for melt-assisted creep

From the above, it is considered very likely that a liquid layer of a few nanometers will be present at the grain boundaries in polycrystalline ice that is close to the melting temperature. This in turn provides an efficient pathway for flow via the grain boundaries. If the ice is subjected to a differential stress, then on the grain boundary site at which the largest principal stress is applied, the grain boundary will have the

tendency to close. This will squeeze out the water present at this site of the grain boundary and water will be transported to the sites of the grain boundary where the smallest principal stress is applied. At low stresses, the applied stress squeezes out the liquid layer, a new equilibrium liquid layer will form to lower the interfacial energy at the grain boundary. If the applied stress is high, it squeezes out the liquid layer and the stress on the grain boundary will cause increased melting at the grain boundary. For both mechanisms it results in ice melting at the highly stressed grain boundary, transport through the grain boundary to the site of the grain boundary with a low stress, where it refreezes. The mass flux around individual grains is determined by the kinetics of melting, transport and refreezing and the creep is thus controlled by the slowest of these three serial processes. Hence, polycrystalline ice will flatten in the $\sigma 1$ direction and elongates in the $\sigma 3$ direction. Theoretically, in temperate ice grain boundary transport may attribute to deformation and the observed increase in strain-rate. Since it is undetermined whether the liquid layer is formed by pressure melting or equilibrium pre-melting and whether transport takes place as diffusion or viscous flow this mechanism is best to be called melt-assisted creep. This process can be envisaged as an analogue of pressure solution creep in rocks, the difference being that, in this case, grain boundary melting creates its own fluid.

Introducing a flow law for temperate ice based on the mechanism of melt-assisted creep helps to improve our understanding of the rheological behavior of (temperate) ice sheets. The increase in computational power over the last decades have made numerical models increasingly important in studying ice sheets dynamics. However, the accuracy of model predictions to a large extend depends on the accuracy of input parameter values. The accuracy of underlying rheological ice flow laws is therefore of great importance in establishing accurate predictions. In order to understand the flow of ice sheets it is therefore relevant to understand the deformation mechanism governing flow in temperate ice and to assess if melt-assisted melt creep is taking place, rather than power-law creep (e.g. Glen's flow law) as suggested by experiments showing faster creep in this temperature regime (Mellor and Testa 1969; Duval 1977; Morgan 1991).

3 A theoretical model for melt-assisted creep

Section 2.4.2 shows that there is significant evidence for the existence of fluid films on the grain boundaries of ice and wire regalation experiments (Gilpin 1980) indicate that this layer is of sufficient thickness to sustain viscous flow down to at least 258 K. The thickness of this layer increases rapidly when the ice approaches the melting point (see Figure 10) and this is expected to enhance grain boundary viscous flow, which may in turn enhance strain-rates in ice close to the melting point. The strain-rate caused by this process is expected to be controlled by: (1) melting of ice at a (highly) stressed surface, (2) transport of flow through the grain boundary or (3) (re-)freezing of water at a stress free/low stress surface. The rate of transport is determined by the slowest of these three serial processes in a similar way as pressure solution creep in fault rocks (e.g. Pluymakers and Spiers 2015) or rocksalt (e.g. Spiers and Schutjens 1990). In this chapter, a theoretical derivation is given for each of the three rate-controlling processes, in which axial strain is related to driving stress. For the slowest of the three processes, the model is adjusted for wire regalation in which the (vertical) displacement of the wire is related to the force exerted on the wire.

3.1 A microphysical model for melt-assisted creep in polycrystalline ice

Melt-assisted creep takes place at the grain boundaries of polycrystalline ice. In order to assess this intergranular deformation mechanism, a grain scale model is required which requires some assumptions and simplifications regarding the geometry and distribution. Let us assume that all grains have the same size and have a cylindrical shape with a radius a in which the height is equal to the diameter (h=2a=d) and both are equal to the grain size. In that case, we can narrow down our model to a single cylindrical grain that is subjected to a uniaxial stress at the top surface of the cylinder. At this surface an equilibrium liquid layer is assumed to be present, of which the thickness depends on temperature. For this model it is assumed that there are no variations in thickness of the grain boundary fluid film and any effects of surface roughness are neglected. It is assumed that stress does not result in internal deformation of the grains.

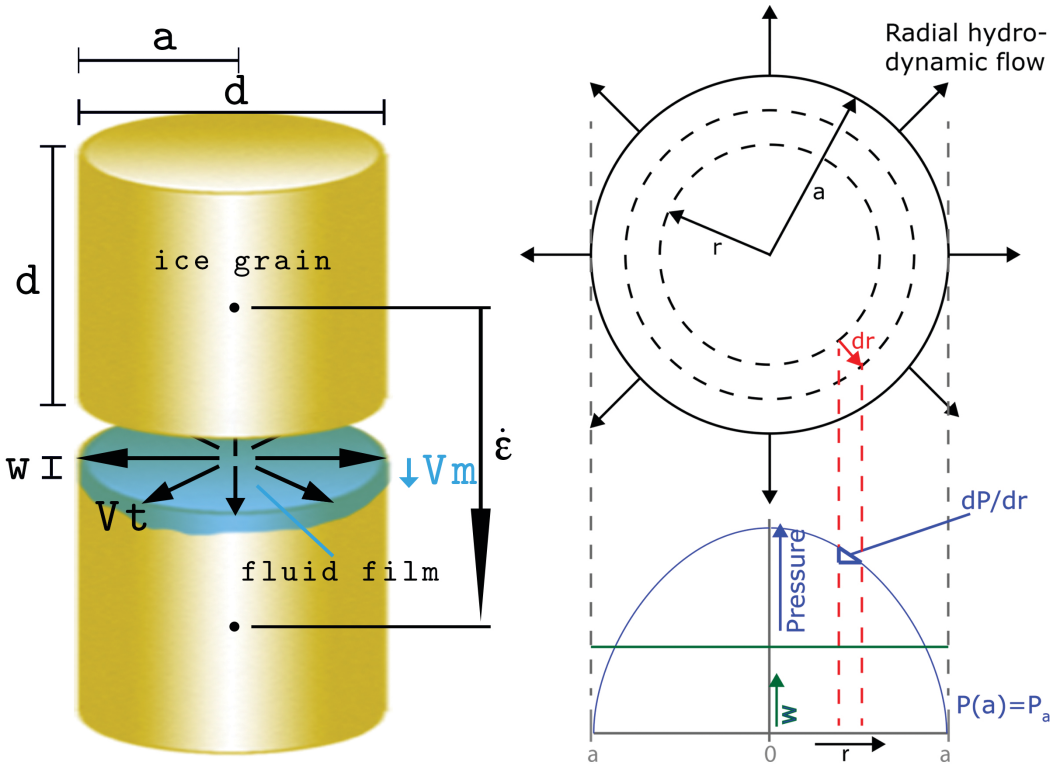

Figure 12: *(a) Schematic drawing of two grains subjected to a uniaxial stress with an equilibrium fluid film in between with a thickness (w). V_t and V_m indicate respectively the velocity of transport due to hydrodynamic radial flow and the velocity of melting. Strain-rate is defined as the rate at which the centers of the two grains approach each other and (b) plan view of contact between the two grains and pressure gradient in the fluid film as a function of radius.*

The stress on the top surface will squeeze out the liquid water to the edge of the cylindrical grain, where it will refreeze. This may occur in pulses, if the melting-rate is very slow compared to the transport-rate, or continuous, if the transport rate is rate-controlling. In that case, the liquid layer can grow faster than it can get squeezed out. Accordingly, it can be approached as having a constant thickness, independent of the dynamics of the model and only on temperature. The amount of melting generated at the top of the cylinder should equal the amount of water transport outwards and the amount of water refreezing at the side of the grain. Hence, mass balance predicts that the following should hold:

$$(\pi a^2) v_{\mathrm{m}} \rho_{\mathrm{ice}} = (2\pi a w) v_{\mathrm{t}} \rho_{\mathrm{w}} = (2\pi a d) v_{\mathrm{f}} \rho_{\mathrm{ice}} \tag{23}$$

in which $\mathrm{v_m}$, $\mathrm{v_t}$ and $\mathrm{v_f}$ are respectively the velocity of melting, transport and refreezing ($\mathrm{ms^{-1}}$), w is the thickness of the fluid film and ρ_{w} and ρ_{ice} are respectively the density of water and ice at 0°C. The velocity of melting governs the velocity at which the centers of two grains are approaching each other and thus gives the (axial) strain rate, when divided by the grain size. However, this does not imply that the process is always controlled by the rate of melting. If the transport or refreezing rates are slower, then the velocity of melting is limited by one of these other processes.

3.1.1 The kinetics of melting and freezing

The melting rate ($\mathrm{v_m}$) is given by the velocity at which the solid-liquid interface boundary moves as a function of chemical potential drop from the solid to the liquid phase ($\Delta\mu$). The Wilson-Frenkel theory (García Fernandez et al. 2006) predicts that the interface response function is given by:

$$v_{\mathrm{m}} = \frac{D_{\mathrm{s}}\delta}{\Lambda^2}(1 - \exp\frac{\Delta\mu}{kT}) \tag{24}$$

In which $\mathrm{D_s}$ is the self-diffusion coefficient represented by the Arrhenius equation $\mathrm{D_s}$=$\mathrm{D_0}$exp $-Q/kT$, Λ is the mean free path for this process and δ is the thickness of the adjacent liquid layer in which diffusion is taking place. $\mathrm{D_0}$ is the pre-exponential diffusion coefficient and Q is the activation energy for grain

boundary diffusion. Measurements on the self-diffusion of ice (Ramseier 1967) show that H^2, H^3 and O^{18} diffuse at almost the same rate (Kuhn and Thürkauf 1958; Ramseier 1967), which suggest that the H_2O molecule diffuses as one unit by vacancy diffusion. Ashby and Verrall (1973) estimated the grain boundary diffusion coefficient by setting $D_s\delta$=D_s2b, in which b is the burger's vector. Ramseier (1967) estimated that the activation energy for grain boundary diffusion to be 0.6 times the activation energy of volume diffusion. The mean free path of a water molecule depends on the amount of empty space in between water molecules and thus depends on the molecular density and the cross-sectional area of a water molecule. The mean free path for a water molecule in its liquid phase is given by:

$$\Lambda = \frac{1}{n\pi(R_{\mathrm{H_2O}})^2} \tag{25}$$

in which n is the Avogadro constant (N_A) divided by the molecular weight of water, which ignoring ^{18}O and ^2H isotopes, is 18 and R_{H_2O} is the spacing between the hydrogen and oxygen, which is about 0.1 nm. The mean free path is therefore 0.25 nm. Using the h=2b approximation of Ramseier (1967), the velocity of melting for small changes in $\Delta\ \mu$ can be written as:

$$v_{\mathrm{m}} = \frac{D_{\mathrm{s}}2b}{\Lambda^2}\frac{\Delta\mu}{kT} \tag{26}$$

or in terms of strain-rate:

$$\dot{\epsilon_{\mathrm{m}}} = \frac{D_{\mathrm{s}}2b}{d\Lambda^2}\frac{\Delta\mu}{kT} \tag{27}$$

The melting rate of ice at the stressed surface is thus controlled by the rate of self-diffusion and the difference in chemical potential between the solid and liquid phase. The term $\frac{D_s2b}{\Lambda^2}$ represents the velocity of melting when $\Delta\mu = kT$. In most theoretical treatments (e.g. Rutter 1976) the difference in chemical potential is given by the difference in (molecular) volume between the solid and liquid phase (ΔV) times the normal stress on the grain boundary (σ_n). The strain-rate for melting controlled melt-assisted creep hence is given by:

$$\dot{\epsilon_{\mathrm{m}}} = \frac{D_{\mathrm{s}}2b}{d\Lambda^2}\frac{\sigma_{\mathrm{n}}\Delta V}{kT} \tag{28}$$

Since the ice can grow onto the existing surface of the sides of the grains (e.g. there is no barrier to nucleation of the ice) and the increase in normal stress at the melting surface is equal to the decrease in normal stress at the freezing surface, the theoretical strain-rate of the freezing step has the same kinetics. The only difference being that the surface area of the side of the cylindrical grain (πd^2) is twice as large as the area of the top surface, so there is twice as much space available for freezing to occur. The strain-rate for freezing in turn is then given by:

$$\dot{\epsilon_{\mathrm{f}}} = \frac{2D_{\mathrm{s}}2b}{d\Lambda^2}\frac{\sigma_{\mathrm{n}}\Delta V}{kT} \tag{29}$$

Interface controlled melt-assisted creep (melting or freezing) theoretically has a linear dependency on stress (n=1) and an inverse linear dependency on grain size (p=1)

3.1.2 The kinetics of transport

The transport of flow through the grain boundary can be envisaged as radial flow in between two circular planes in which a pressure gradient exist due to an externally applied stress (see Figure 12) and can be described as hydrodynamic flow, using the equation of Poiseuille (Equation 30), which is a solution of the Navier-Stokes equation for an in-compressible fluid of uniform and constant viscosity (Batchelor 1967). Poiseuille's flow only holds when the liquid layer is thick enough to have a viscosity which is close to the bulk viscosity of water. Israelachvili (1986) and Chan and Horn (1985) show that bulk values for viscosity of liquids is manifest down to the last single or two molecular layers at the surface. Using Poiseuille's flow, the average velocity in between the two plates is given by:

$$v_{\mathrm{t}} = \frac{w^2}{12\eta_{\mathrm{eff}}(T,w)}\Big(\frac{-dP}{dr}\Big) \tag{30}$$

in which w is the width of the grain boundary fluid film η is the viscosity of water and dP/dr is the pressure gradient driving flow in the grain boundary. Mass balance predicts that the following should hold:

$$(\pi r^2)v_{\mathrm{m}}\rho_{\mathrm{ice}} = (2\pi rw)\Big[\frac{w^2}{12\eta_{\mathrm{eff}}(T,w)}\Big(\frac{-dP}{dr}\Big)\Big]\rho_{\mathrm{w}} \tag{31}$$

which can be rearranged and rewritten such that an equation can be obtained for the change in pressure as a function of the radial coordinate from the the centre of the top surface of the cylindrical grain (r), which yields:

$$dP(r) = -6(v_{\mathrm{m}})\Big[\frac{\rho_{\mathrm{ice}} * \eta_{\mathrm{eff}}(T,w)}{\rho_{\mathrm{w}} * w^3}\Big] * r \tag{32}$$

where $6(v_{\mathrm{m}})\Big[\frac{\rho_{\mathrm{ice}}*\eta}{\rho_{\mathrm{w}}*w^3}\Big]$ can be combined as a constant K. If we now integrate this function we obtain an equation for pressure in the grain boundary water in between r=0 and r=a (see Figure 12). The pressure is then given by:

$$P(r) = \frac{K}{2}(a^2 - r^2) + P_{\mathrm{a}} \tag{33}$$

in which $\mathrm{P_a}$ represents the boundary condition of the pressure at the edge of the disk. At the same time there should be a force balance between the external stress applied on the top of surface the cylinder and the pressure at any point in the fluid withstanding this stress. Mathematically speaking this implies that the integrated pressure curve between r=0 and r=a must equal the total stress on the surface, hence the following should hold:

$$\sigma\pi a^2 = \int_0^a P(r)2\pi r dr \tag{34}$$

Solving this integral and dividing both sides by π and a, gives us an equation for stress, which can be written as:

$$\sigma = \frac{Ka^2}{4} + P_{\mathrm{a}} \tag{35}$$

using $K = 6(v_{\mathrm{m}})\Big[\frac{\rho_{\mathrm{ice}}*\eta}{\rho_{\mathrm{w}}*w^3}\Big]$ and rearranged we can obtain an equation for effective stress:

$$\sigma - P_{\mathrm{a}} = \frac{3}{2}(v_{\mathrm{m}})\Big[\frac{\rho_{\mathrm{ice}} * \eta_{\mathrm{eff}}(T,w)}{\rho_{\mathrm{w}} * w^3}] * a^2 \tag{36}$$

Rearranging equation 36 for $\mathrm{v_m}$ and using $\dot{\epsilon} = v_{\mathrm{m}}/2a$ gives the stress-strain relationship for transport controlled pressure induced melt creep, yielding:

$$\dot{\epsilon_{\mathrm{t}}} = \frac{\rho_{\mathrm{w}} * w^3}{3\rho_{\mathrm{ice}} * \eta_{\mathrm{eff}}(T,w)} * \frac{\sigma - P_{\mathrm{a}}}{a^3} \tag{37}$$

The term $\sigma - P_{\mathrm{a}}$ can be envisaged as the effective stress on the grain boundary. For uniaxial compression at atmospheric pressure, the pressure in the fluid at the edge of the top surface ($\mathrm{P_a}$) is expected to be 0 and the applied stress is equal to the effective stress. Assuming an equidimensional grain, the vertical length is equal to the diameter. Hence the vertical d is equal to 2 times the radius (a) (see Figure 12). Therefore, in terms of grain size (d) the strain-rate can be expressed as:

$$\dot{\epsilon_{\mathrm{t}}} = \frac{8}{3}\frac{\rho_{\mathrm{w}} * w^3}{\rho_{\mathrm{ice}} * \eta_{\mathrm{eff}}(T,w)} * \frac{\sigma}{d^3} \tag{38}$$

ρ_{ice} is constant and ρ_{w} only slightly decreases in between 273 and 258 K, so 39 can be rewritten and rearranged, such that:

$$\dot{\epsilon_{\mathrm{t}}} = A\frac{w^3(T)}{\eta_{\mathrm{eff}}(T,w)} * \frac{\sigma}{d^3} \tag{39}$$

in which A=2,91. Equation 39 shows that transport controlled melt-assisted creep is linear dependent on effective stress (n=1) and has an inverse cubic dependence on grain size (p=3). This equation shows that it is very sensitive to the thickness of the fluid film ($\dot{\epsilon} \propto w^3$).

3.2 A microphysical model for wire regalation

The model for transport controlled melt-assisted creep can be rewritten for the flow of an equilibrium liquid layer between a loaded wire and ice (see Figure 13). This model assumes no pressure melting occurs. In that case, the liquid layer is in equilibrium and regalation is expected to be limited by the viscous flow in the liquid layer (slow regalation mode in the terminology of Gilpin (1979). If pressure melting occurs, the stress of the wire causes lowering of the internal temperature of the ice and causes out-of-equilibrium melting and the thickness of this liquid layer increases and conductivity through the wire becomes rate-limiting (fast regalation mode in the terminology of Gilpin (1979). This fast regalation mode is beyond the scope of this study as it can not be used to study the equilibrium layer. In this model it is assumed that the vertical velocity of the wire can be calculated by assuming that the fluid film can be trated as a flat ribbon with a width of 2a and a length L subjected to a normal stress σ. For this model, the difference in transport distance (which is equal to a for the center to the edge of the ribbon and πa for a quarter circle) can be neglected.

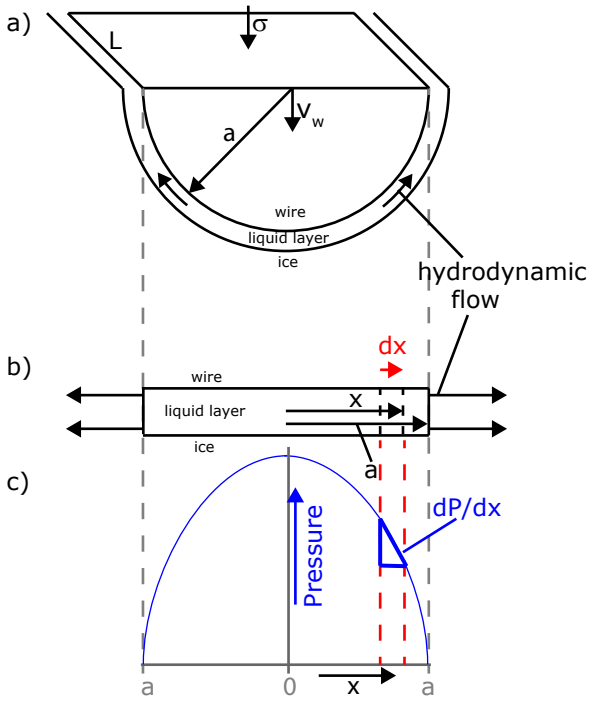

Figure 13: *(a) schematic drawing of a liquid layer in between a loaded wire and ice, (b) simplified ribbon model for hydrodynamic flow in the liquid layer between a wire and ice and (c) pressure gradient in the liquid layer due to externally applied stress on the wire.*

Using the same approach as for the cylindrical grain-to-grain model, a mass balance can be obtained, which yields:

$$Lxv_{\mathrm{w}}\rho_{\mathrm{ice}} = Lw\left[\frac{w^2}{12\eta_{\mathrm{eff}}(T,w)}\left(\frac{-dP}{dx}\right)\right]\rho_{\mathrm{w}} \tag{40}$$

In which v_w is the velocity of the wire in ms^{-1}, x is the distance from the center of the ribbon and L is the length of the wire. Since L appears on both sides the problem reduces to a 2D problem. Rearranging equation 40 for dP and taking the integral of this function gives the equation for pressure, which results in:

$$P(r) = \frac{K}{2}(a^2 - x^2) + P_{\mathrm{a}} \tag{41}$$

in which K is $12(v_{\mathrm{w}})\left[\frac{\rho_{\mathrm{ice}} * \eta}{\rho_{\mathrm{w}} * w^3}\right]$. The pressure in the liquid layer between 0 and a should be equal to the externally applied stress, hence the force balance can be expressed as follows:

$$\sigma a = \int_0^a P(x)dx \tag{42}$$

Solving this integral results in the following expression for stress:

$$\sigma = \frac{Ka^2}{3} + P_{\mathrm{a}} \tag{43}$$

in which P_a is assumed to be 0 as the pressure in the liquid layer goes to 0 at the edge of the wire. If we substitute K back into equation, then the equation can be rewritten, such that:

$$\sigma = 4v_{\mathrm{w}}\Big[\frac{\rho_{\mathrm{ice}} * \eta_{\mathrm{eff}}(T,w)}{\rho_{\mathrm{w}} * w^3}\Big] * a^2 \tag{44}$$

This equation can be rearranged for v_w and in terms of wire diameter (d_{wire}) the equation for wire regalation velocity can be written as:

$$v_{\mathrm{w}} = \frac{\rho_{\mathrm{w}}}{\rho_{\mathrm{ice}}}\frac{w^3}{\eta_{\mathrm{eff}}(T,w)} * \frac{\sigma}{{d_{\mathrm{wire}}}^2} \tag{45}$$

in which ρ_w/ρ_{ice} can be combined as constant A, which gives:

$$v_{\mathrm{w}} = A\frac{w^3}{\eta_{\mathrm{eff}}(T,w)} * \frac{\sigma}{{d_{\mathrm{wire}}}^2} \tag{46}$$

in which A$\sim$1.09. Using this equation it is possible to experimentally derive the fluid film thickness by measuring the wire regalation velocity at different temperatures. Wire regalation experiments can also be used to validate if the velocity has a stress-exponent of n=1 and an inverse dependence on wire diameter of 2. Gilpin (1979) shows the same relation to stress and wire diameter as the wire regalation model derived in this study, but heir derivation leads to a constant A of 0.25. A comparison between the model for wire regaltion velocity derived in this study and the model of Gilpin (1979) is given in section 5.1.1.

3.3 Results of microphysical model for polycrystalline ice

One of the aims of the model was to provide a theoretical basis for melt-assisted creep and obtain an equation that relates the strain-rate of a cylindrical grain as a function of applied stress, in which the rate is controlled by melting, freezing or transport. In the previous section, equations have been derived for melting/freezing controlled strain-rates (Equation 28 & 29) and for transport-controlled strain-rates (Equation 39) in polycrystalline ice. These equations can be expressed in terms of varying conditions of stress, grain-size and temperature. The transport-controlled creep rates also depends on the fluid film thickness. The thickness of the liquid layer (w), can not be predicted by our model as it finds its origin in lowering of the surface energy and has a thermodynamic basis. Therefore, the equations of Gilpin (1979) and Fletcher (1973) are used (Equation 20 & 19) as input for the fluid film thickness as a function of temperature, as well as exploring the effect of an immobilized layer on the effective viscosity. In this section, the strain-rates for this theoretical model for melt-assisted creep in polycrystalline ice are presented for: (1) small grain sizes at which this mechanism is expected to become more important (0.1 to 10 mm), (2) stresses that occur naturally in ice sheets (0.01-1 MPa) and (3) temperatures close to the melting point.

3.3.1 Rate-controlling mechanism of melt-assisted creep in polycrystalline model

The equations for the strain-rate, if melt-assisted creep is controlled by melting (Equation 29) or by transport (Equation 39) are shown as a function of stress (see Figure 14) and grain-size (see Figure 15). These figures show that the transport rate is at least 4-5 magnitudes smaller than the melting rate. At larger grain-sizes, the difference becomes even larger and there are no naturally occurring conditions at which the melting-rate becomes slower (and hence rate-controlling). Therefore, melt-assisted creep will always be controlled by transport through the grain boundary and the strain-rate is determined by Equation 39.

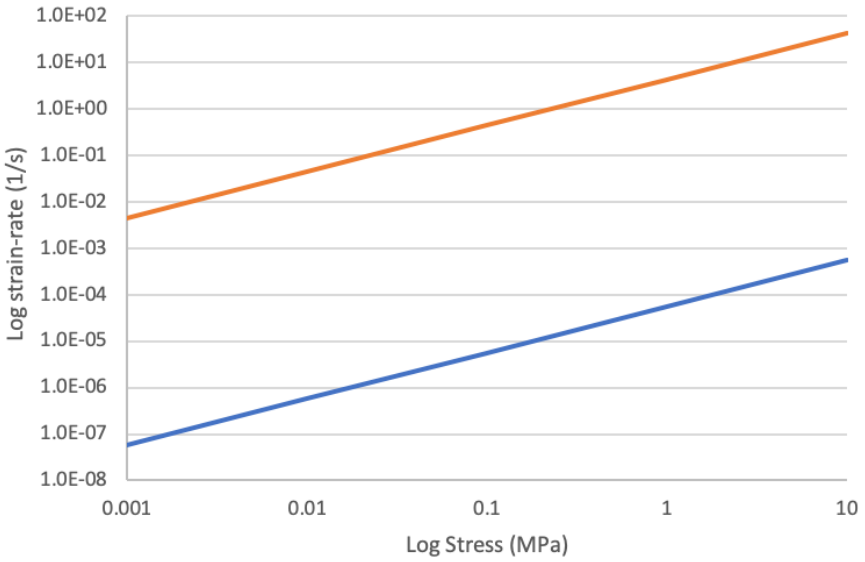

Figure 14: *Melting-rate (Equation 29) (orange line) and transport-rate (Equation 39) (blue line) for the as a function of stress at a constant temperature (272 K) and a grain-size of 0.1 mm in polycrystalline model. This shows that the transport step is rate-limiting over the complete range of stress.*

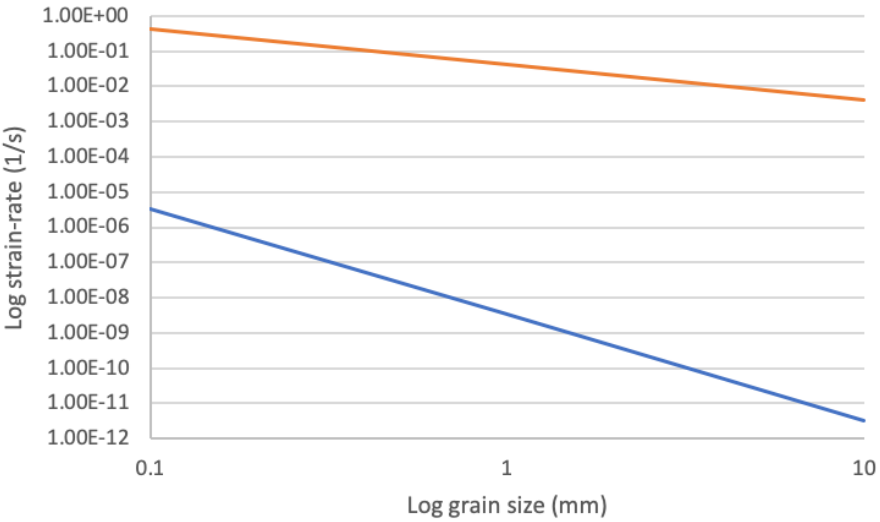

Figure 15: *Melting-rate (Equation 29) (orange line) and transport-rate (Equation 39) (blue line) as a function of grain size at a constant temperature of 272 K and stress of 0.1 MPa in polycrystalline model. This shows that the transport step is rate-limiting over the complete range of grain size.*

3.3.2 The effect of fluid film thickness and an immobile layer on strain-rates

In section 2.4.1, two different equations for the fluid film thickness have been presented: (1) Equation 20, which is inferred from wire regalation measurements at different temperatures, which is given by:

$$w = 3,5(-T)^{1/2.4}$$

in which T is in degrees Celsius and (2) Equation 19 which is based on thermodynamic calculations of lowering the surface energy and is given by:

$$w = C - 2,5log(-T)$$

where C is a constant between 2 and 5 nm and T is the temperature in degrees Celsius. Because the Equation of Gilpin (1979) is a good average of the upper and lower bound of the model of Fletcher (1973), the next calculations all use the equation of Gilpin (Equation 20) as input for fluid film thickness (w) in equation 39.

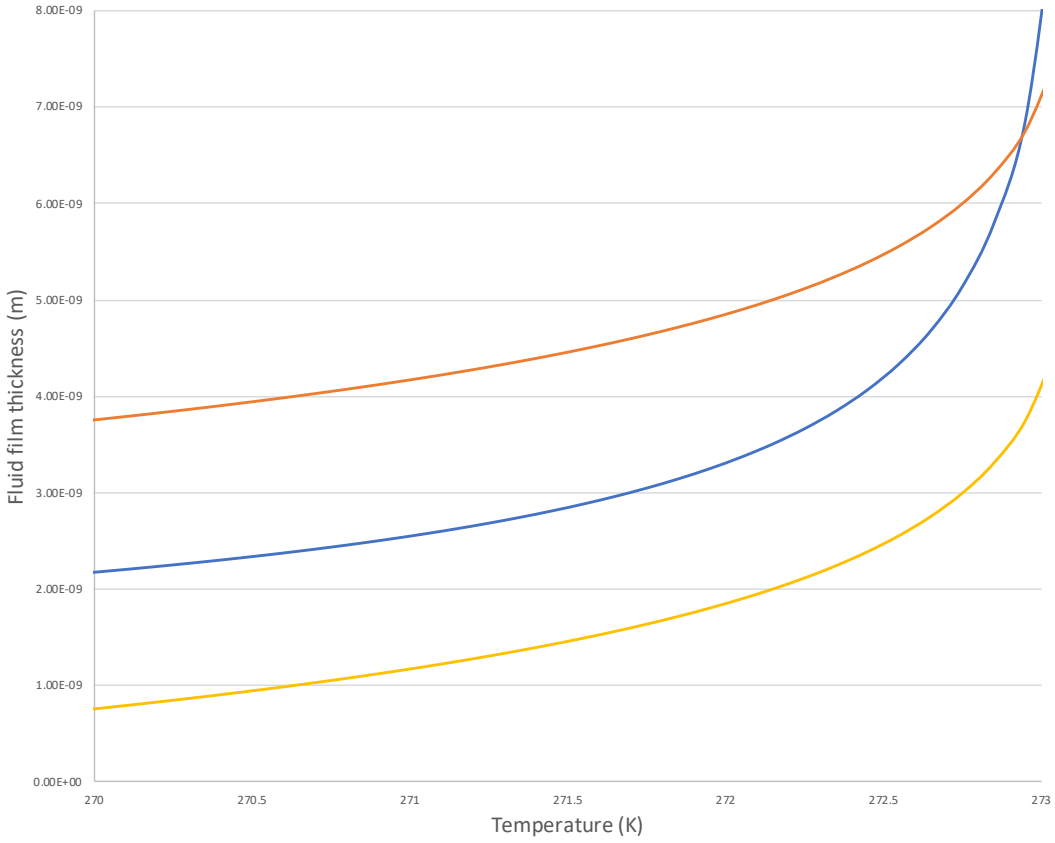

Figure 16: *Fluid film thickness (w) as a function of temperature for $w = C - 2,5log(-T)$ (Gilpin 1979) and $w = C - 2,5log(-T)$ (Fletcher 1973). Gilpin (1979) model is indicated by blue and Fletcher (1973) model is indicated by respectively orange for the upper bound (C is 5 nm) and yellow for the lower bound (C is 2 nm).*

As previously discussed it is not very likely that the complete fluid film is mobile. Up to 2 layers of H_2O-molecules may be immobilized at the surface of the grain boundaries on the top and bottom side. This causes a decrease in effective thickness and an increase in effective viscosity. The effect of such an immobile layer on strain-rate is shown in Figure 17. When an immobile layer of 0.86 nm is presents, viscous flow is impossible below ~268 K. However, the effects of such a thick immobilized layer are relatively small when the temperature approaches the melting point. The highest strain-rates predicted by melt-assisted creep for temperate ice at these conditions are in the order of 10^7 s^{-1}.

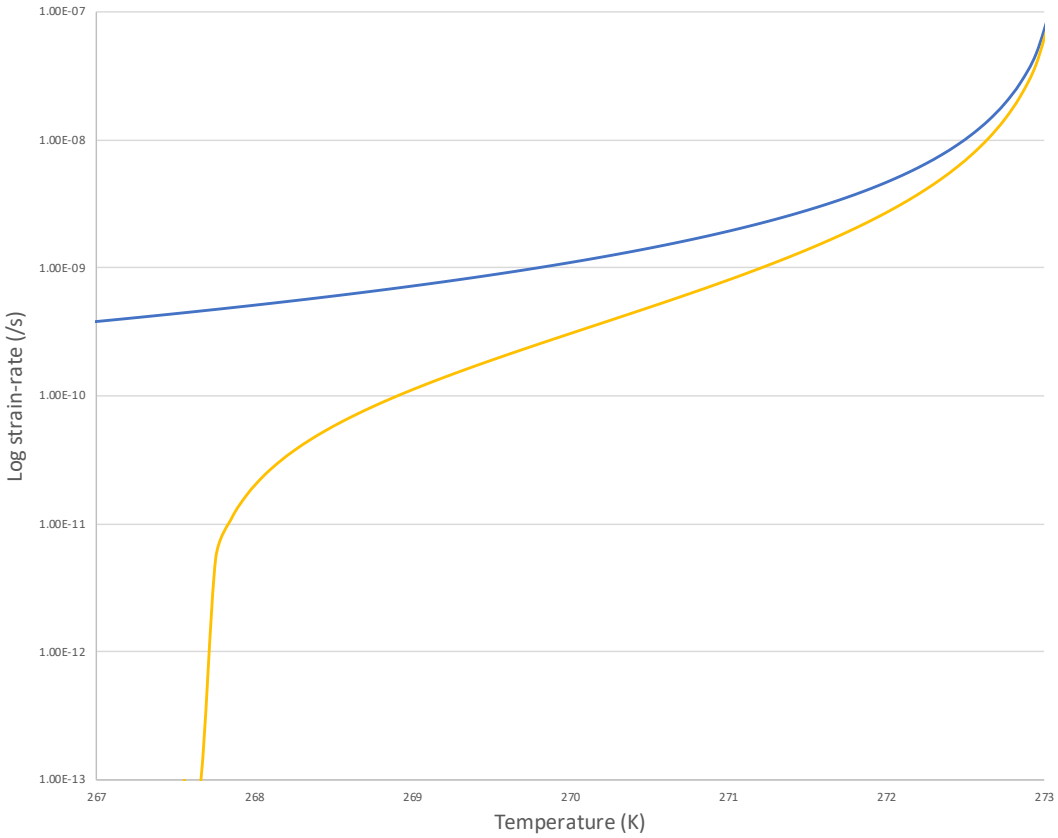

Figure 17: *Strain-rates showing the effect of an immobile layer attached to either side of the grain boundary. The grain size and stress for this run are respectively 1 mm and 0.1 MPa. Blue line shows strain-rate for an immobile layer of 0.275 nm (1 layer of immobilized H2O molecules) and yellow line shows strain-rate for an immobile layer of 0.86 nm (2 layers of immobilized H2O molecules with an H-bond).*

3.3.3 The effect of grain size, stress and temperature on strain-rates

The strain-rates predicted from our polycrystalline model are increasingly high near the melting point. Therefore, the strain-rates as a function of grain size and stress for T=270-273 K are shown in respectively Figure 18 and Figure 19.

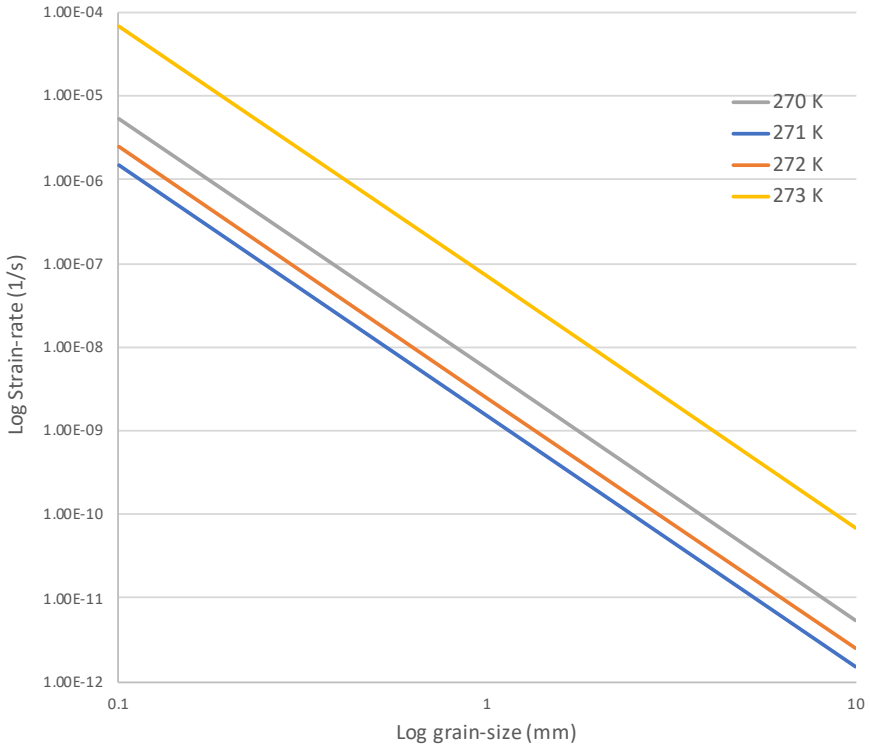

Figure 18: *Strain-rate as a function of grain-size for different temperature curves of 270 K to 273 K (at a constant stress of 0.1 MPa).*

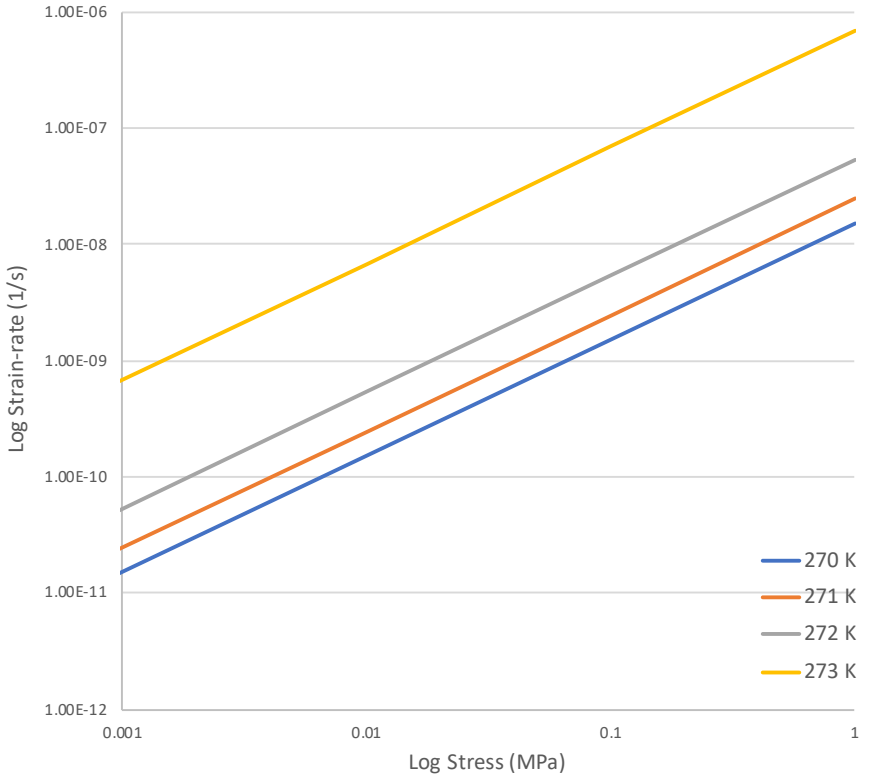

Figure 19: *Strain-rate as a function of stress for different temperature curves of 270 K to 273 K (at a grain-size of 1 mm).*

3.4 Results of microphysical model for wire regalation

The other aim was to provide a theoretical basis for wire regalation and obtain an equation that relates the velocity of the wire as a function of applied stress, wire diameter and temperature. In the previous section, equations have been derived for transport-controlled wire regalation velocities (Equation 46). Wire regalation velocities results are presented for a wire diameter of 25-100 $/mu$m, stress ranging from 0.1 to 10 MPa and high temperatures (270-273 K). Predictions on the velocity of the wire can be done based on Equation 46. The fluid film thickness again is based on Equation 20 from Gilpin (1979). For these results it has been chosen to not use an immobile layer, which makes it possible to compare results to the wire regalation experiments of Gilpin (1980), as he also assumed bulk viscosity (Equation 22). The results are presented for a wire diameter of 25-100 μm, stress ranging from 0.1 to 10 MPa and high temperatures (270-273 K). These conditions are chosen such that the wire is sufficiently strong to support the load and that displacement velocities are readily measurable $>1\mu$m/hr.

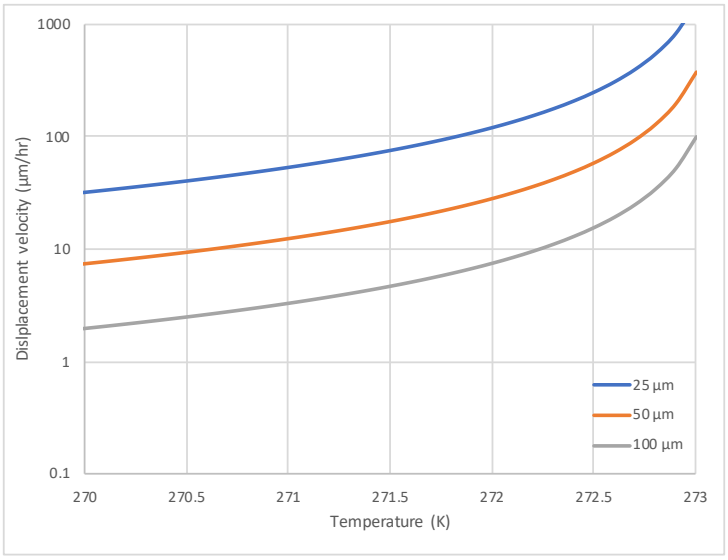

Figure 20: *Displacement velocity as a function of temperature for wire diameters of 25 µm (blue), 50 µm (orange) and 100 µm (grey).*

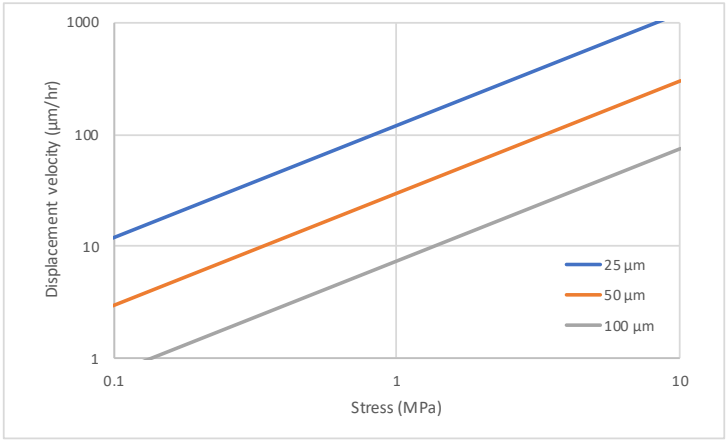

Figure 21: *Displacement velocity as a function of stress for wire diameters of 25 µm (blue), 50 µm (orange) and 100 µm (grey).*

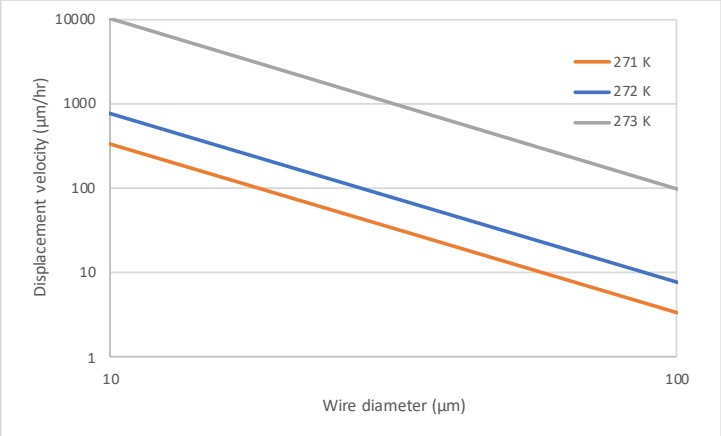

Figure 22: *Displacement velocity as a function of wire diameter for temperatures of 271 K (orange), 272 K (blue) and 273 K (grey).*

4 Wire regalation experiments conducted here

The aim of performing wire regalation experiments was to test if the model for wire regalation derived in section 3.2 accurately describes the wire regalation velocity. The main goal was to validate the stress-exponent (n=1) and "wire diameter" exponent (p=2) in the wire regalation model.

$$v_{\mathrm{w}} = A\frac{w^3}{\eta_{\mathrm{eff}}(T,w)} * \frac{\sigma}{{d_{\mathrm{wire}}}^2}$$

4.1 Method

Wire-regalation experiments were performed by the apparatus shown in Figure 23. The cylindrical ice sample had a diameter of 20 mm and was placed on a table in a ring to keep it stable. The wire was connected to a frame and could be put under tension to minimize deflection of the wire. Two types of wires were chosen to perform the experiments: 360L stainless steel and Tungsten wire. The frame was connected to a weight and a Linear velocity displacement transducer (LVDT) to measure vertical displacement and the frame could move freely in the vertical direction. The unloaded frame had a weight of 16,68g and a total weight of up to ∼300g could be added, hence up to 3 N of force could be applied. This made it possible to perform experiments in the range of 0.3-2 MPa depending on the diameter of the wire. The temperature was measured by two pt100 sensors, one located in the saline/ice water bath and one adjacent to the ice sample. The apparatus was placed in a water-tight cylinder, which in turn was placed in a saline ice/water buffer in a steel box surrounded by a polystyrene box. At the top of the water-tight cylinder a steel pipe was made to lead the wires for the pt100 temperature sensor and the LVDT. The space next to these wires was filled with insulation to minimize cold loss. The salinity of the ice/water bath was chosen such that the desired freezing point depression matched the desired experimental temperature, using Equation 47 for freezing point depressions for H_2O-NaCl solutions of Hall et al. (1988).

$$salinity = 1,78(-T) - 0,042(-T)^2 + 0,000557(-T)^3 \tag{47}$$

in which salinity is in weight percentage (wt. %) and T is in °C. Ice samples were grown by freezing distilled water using a domestic freezer at 255 K. The ice samples were taken out of the freezer after 2 hours and put in the apparatus. It was not possible to let the sample equilibrate before the start of the experiment as the frame could not be handled from outside of the container and the wire was immediately lowered to the surface to start the experiments. However, it was expected that the temperature in the water-tight container would quickly go back to the temperature of the surrounding saline/ice water bath and that the surface of the ice sample, hence the contact between the wire and the ice, quickly would go to the desired experimental temperature and a steady-state would be reached.

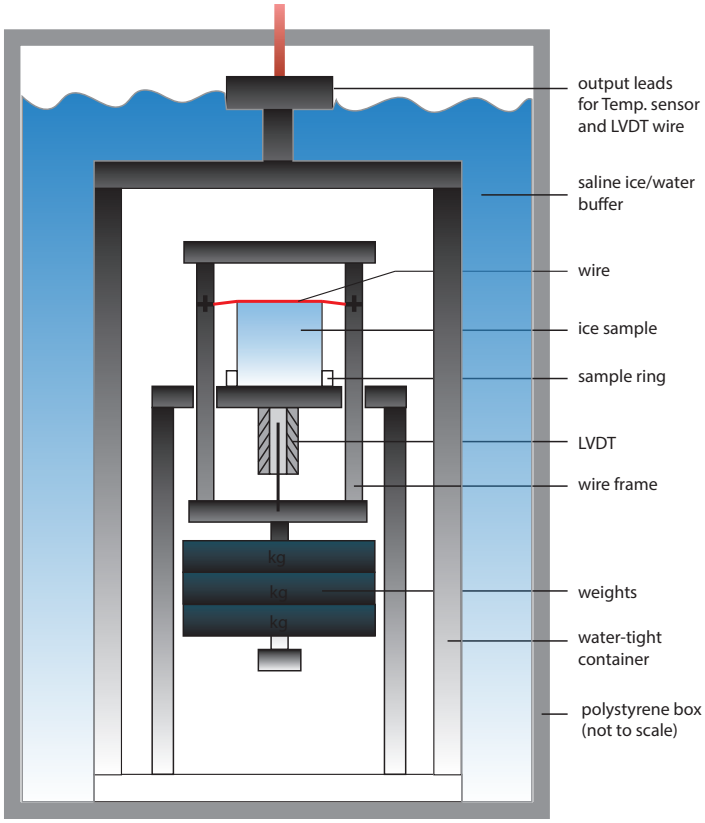

Figure 23: *Schematic diagram showing the wire regalation apparatus*

4.2 Results

An attempt was made on performing wire regalation experiments. Figure 24 shows the difference in temperature between the saline ice/water mixture and the air temperature in the cylinder adjacent to the ice sample.

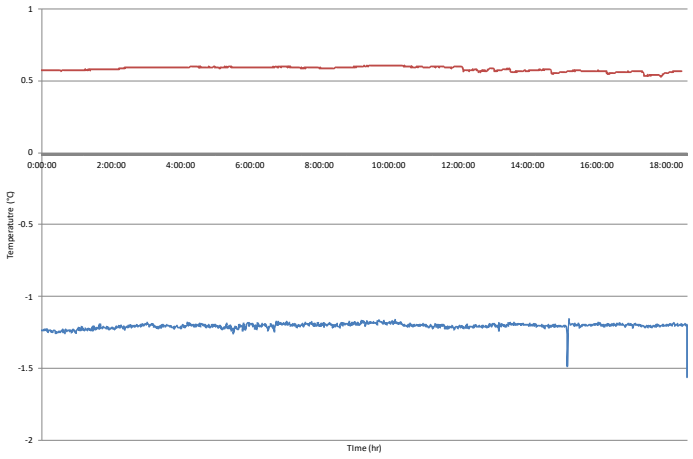

Figure 24: *Temperature test of experimental setup. Red line indicates temperature of the air adjacent to the ice sample and blue line indicates saline ice/water buffer temperature.*

Using a hose pump, the still standing air in the top part of the cylinder could be mixed with the lower part and the hoses were directed through saline water to make sure the temperature would reach a constant temperature. The temperature of the saline water needed to be about 1 K colder as the desired temperature. Using this setup and a wire diameter of 80 μm at a stress of 1 MPa and a temperature

of -1.1°C a wire regalation experiment was performed (see Figure 25). The vertical displacement of the frame was recorded to be 17 μm/hr.

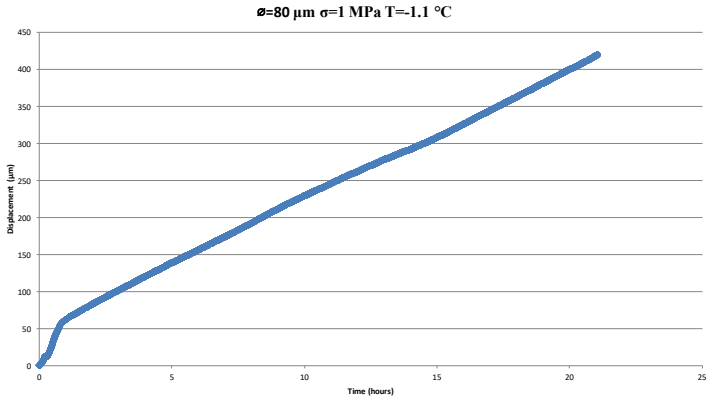

Figure 25: *Present regalation experiments showing displacement of the wire as a function of time for a wire with a diameter of 80 μm, loaded with 163g (including frame weight: 1 MPa) at a temperature of -1.1 °C. Steady-state velocity of 17 μm/hr.*

5 Discussion

Here, the results of the wire regalation experiments are discussed. Subsequently, the theoretical model for wire regalation derived in this study is compared to the wire regalation theory of Gilpin (1979) and compared to experimental wire regalation data. The results of the model for melt-assisted creep in polycrystalline ice are then discussed in the context of other (GSS) deformation mechanisms and compared to data from creep experiments on polycrystalline ice. Finally, it is discussed whether there is evidence for this mechanism occurring in ice sheets and what the implications of this mechanism will be on creep rates and ice sheet dynamics.

5.1 Wire regalation experiments

The aim of the wire regalation experiments was to: (1) test whether the displacement of the wire could accurately be described by our model, (2) to infer the thickness of the liquid layer around the wire, (3) to test if the velocity of the wire could be described as having a linear dependency on stress (n=1) and an inverse squared dependency on wire diameter (p=2) and (4) to extrapolate the experimental results to the model for melt-assisted creep. These experiments required a very accurate control on temperature. In order to get readily measurable velocities the temperature should be within 1 K of the melting temperature (see Figure 20) and the variations in temperature preferably should be small. Large variations in temperature would cause large variations in the equilibrium thickness of the fluid film (e.g Equation 19 & 20) and no sensible results would be acquired. A difference of 1.5 K in temperature between the environment in the cylinder (where the apparatus was placed) and the cooling vessel around the cylinder was observed. This posed an issue as it was hoped that equilibrium was reached at which both had the same temperature. A possible solution for this problem was provided by using a hose pomp to circulate cold air through the cylinder, however this caused sublimation of the ice sample surface. The wire regalation velocity of 17 /*mu*m/hr recorded in Figure 25, therefore was in a large part a result of the sublimation of the surface and not the wire cutting through the ice as dimensions of the sample changed during the experiment and it could be observed that the wire was still on the surface. The velocity was 2-8 times higher as expected from the model. Hence, it was not possible to accurately control the conditions and no sensible results were produced.

5.1.1 Comparison with previous work on wire regalation theory

The absence of experimental results makes it impossible to assess whether the wire regalation model of this study accurately describes the velocity of a wire as a function of stress, wire diameter and temperature. However, previous research has been conducted on wire regalation (e.g. Telford and Turner 1963; Drake and Shreve 1973; Gilpin 1979, 1980) which can be used to check the model for wire regalation.

Gilpin (1979) provide a theory for wire regalation based on viscous flow through the liquid layer around the wire.Gilpin (1980) performed experiments to test this theory and to infer the fluid film thickness. His derivation is based on viscous flow around a cylinder on its side instead of around a flat ribbon, resulting in a longer flow path (quarter circle = $1/2\pi$a instead of half the ribbon width = a) and the boundary condition for pressure at the edge of the fluid film (P_a in Section 3.2) is not set to zero, resulting in a smaller pressure gradient. According to his derivation, the velocity of the wire can be described using:

$$v_w = \frac{1}{12\pi}\left(\frac{V_s}{V_l}\right)^2 \frac{w^3}{\eta_{eff}(T)} * \frac{1}{a^3}\frac{F}{L} \tag{48}$$

in which V_s and V_l are respectively the molecular volume of the solid (ice) and liquid (water) and F is the force on the wire. In order to compare this to the model described in Section 3.2, this equation can be rewritten as a function of stress using $F = \sigma/2aL$ (see Figure 13). Using d_{wire}=2a, it can be shown that:

$$v_w = \frac{2}{3\pi}\left(\frac{V_s}{V_l}\right)^2 \frac{w^3}{\eta_{eff}(T)} \frac{\sigma}{{d_{wire}}^2} \tag{49}$$

in which V_s and V_l are constants, hence the equation can be written in the same form as Equation 46, such that:

$$v_w = A\frac{w^3}{\eta_{eff}(T)} \frac{\sigma}{{d_{wire}}^2} \tag{50}$$

in which constant A=0,25. This derivation predicts the same stress (n=1) and wire diameter (p=2) relation as the derivation in this study (see Section 3.2), but A in this study is 4.3 times larger. Rewriting this equation gives an equation in which the fluid film thickness can be inferred at different temperatures, such that:

$$w = \frac{V_w \eta_{eff}(T)}{\sigma} \frac{{d_{wire}}^2}{A} \tag{51}$$

Figure 27b confirms that the velocity can be described by a stress-exponent of n=1. Although not explicitly tested, the fact that Equation 51 can be used to fit experimental data obtained for a broad range of wire diameters (12μm - 380 μm) confirms that this mechanism indeed has an inverse squared dependency on wire diameter (p=2) (see Figure 27a). The predictions on wire velocity of the model in this study and those of Gilpin (1979) are shown in Figure 26.

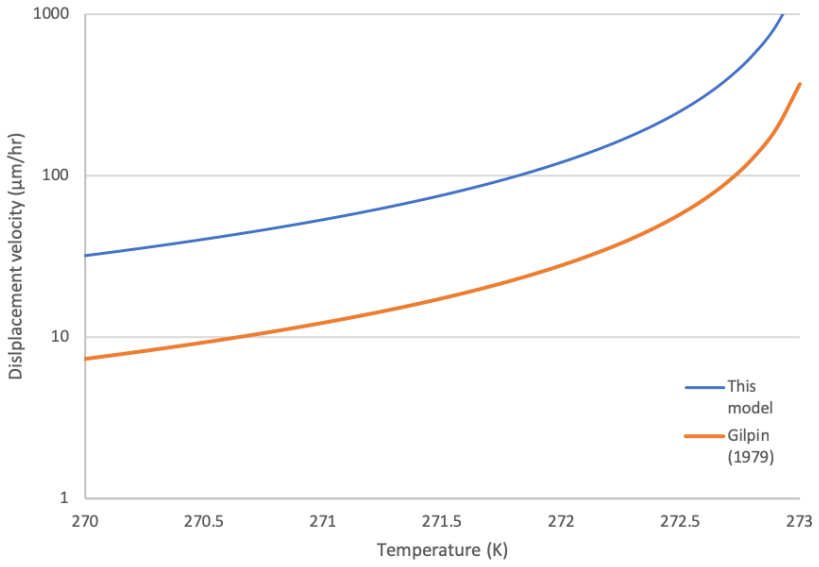

Figure 26: *Wire regalation velocity predicted by the model in this study (blue) and Gilpin (orange) (Equation 50), both use Equation 20 as input for fluid film thickness.*

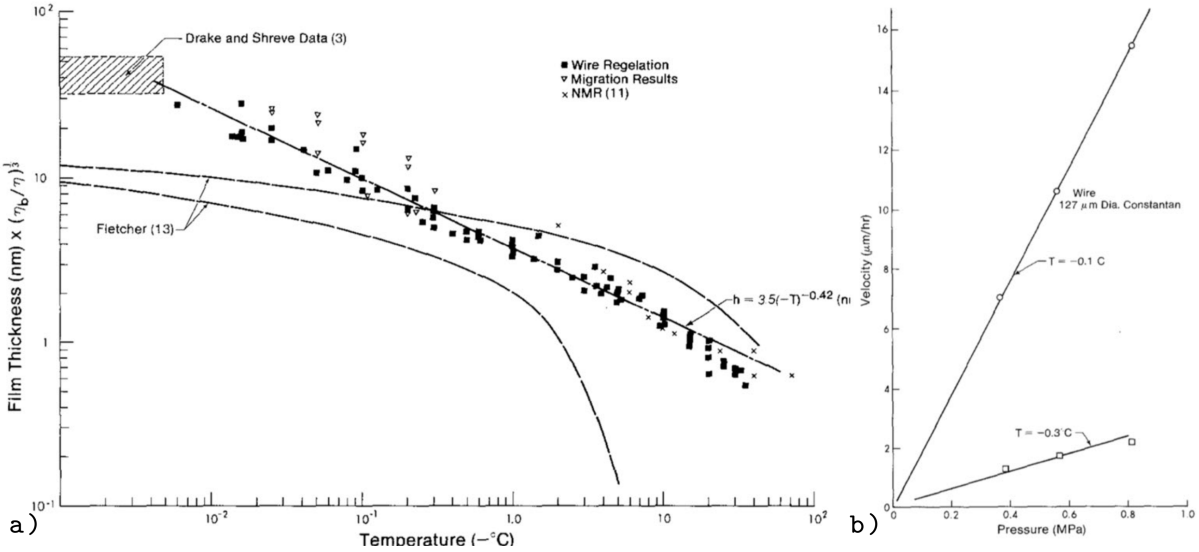

Figure 27: *Experimental data on wire regelation of Gilpin (1980), showing: (a) wire regelation velocity (V_w) data plotted as fluid film thickness (corrected for the change in effective viscosity with temperature (Equation 22), using Equation 51 and (b) wire regelation velocity as a function of applied stress, showing linear (n=1) behavior at T=-0.1°C and -0.3°C.*

The difference between the two models may seem substantial, but there is a high uncertainty on the exact value of the fluid film thickness (w) (see Figure 16) and to fit our model with the experimental data of Gilpin (1980) only requires a slightly lower estimation (factor 0.7) of the fluid film thickness, which is still within the range predicted by Fletcher (1968) (e.g. Equation 19). Thus, to fit our model with the experimental data of Gilpin (1980) would require a modification of Equation 20 ($w = 3.5(-T)^{1/2.4}$), which would then become:

$$w = 2.5(-T)^{1/2.4} \tag{52}$$

This suggest that our model implies an equilibrium thickness of 2.5 nm at -1°C instead of 3.5 nm as inferred by Gilpin (1980).

5.2 Experimental evidence for melt-assisted creep in the literature

In this thesis, only a model is presented for melt-assisted creep and no creep experiments on polycrystalline ice were performed to: (1) see if this mechanism actually occurs, (2) test whether the strain-rates predicted by this model are of the same magnitude as observed in experiments, (3) check if creep experiments show the same stress and grain size exponent as predicted by our model and (4) if the relation with temperature (and hence the predicted fluid film thickness) is correct. In this section, data from creep experiments is used to assess whether there is evidence for melt-assisted creep and if previous research has observed the stress and grain size exponent predicted by this model.

5.2.1 Melt-assisted creep compared to other GSS mechanisms in ice

It is widely accepted that when stress is high (>1 MPa), grain sizes are large (>10mm) and the ice is cold (<268), the internal deformation of the ice can be described reasonably well by power-law creep (see Table 2), such as Glen's flow law, and dislocation creep is the main deformation mechanism (e.g. Glen 1955; Paterson 1994). At low stresses, there is a clear indication of a decrease in stress-exponent (e.g Steinemann 1954; Mellor and Testa 1969; Colbeck and Evans 1973; Schulson and Duval 2009a; Goldsby and Kohlstedt 2001). For a long time it was difficult to obtain convincing results in the laboratory and there was no consensus on the deformation mechanism and the corresponding stress-exponent at low stress. Goldsby and Kohlstedt (1997, 2001) were able to perform experiments on very fine grained polycrystalline ice, showing that (at low stress, for small grain sizes), deformation can be described by a stress-exponent of 1.8 and a grain size exponent of 1.4 (see Figure 7) and ascribed this to deformation

by GBS accommodated by basal slip. They show that deformation of ice at low stresses can be fitted, using:

$$\dot{\epsilon} = A_{\mathrm{GBS}} \frac{\sigma^{1.8}}{d^{1.4}} exp\Big(\frac{-Q}{RT}\Big) \tag{53}$$

in which the values for A and Q are listed in Table 4. A solution of this empirical equation as a function of temperature is shown in Figure 28. These experiments seem to indicate that there is no evidence for diffusion, which would have a stress-exponent of n=1 and such linear behavior is not observed even at the lowest stresses (Goldsby and Kohlstedt 2001). Equation 18 can be used to assess the theoretical contribution of diffusion at similar conditions. Equation 18 can be rewritten, such that diffusional strain-rates are given by:

$$\dot{\epsilon} = \frac{42\sigma V_{\mathrm{m}}}{RTd^2}\Big(D_{\mathrm{v}} + \frac{2b\pi}{d} D_{\mathrm{gb}}\Big) \tag{54}$$

in which V_m is the molar volume of the solid (m^3mol^{-1}). The diffusion coefficients (D_v and D_{gb}) are each of the form $D=D_0\exp(\frac{-Q}{RT})$ and the grain boundary width (δ) is 2b, according to the same reasoning as in section 3.1.1. The pre-exponential terms ($D_{0,v}$ and $D_{0,gb}$) are based on the approximations of Ramseier (1967), which are also discussed in section 3.1.1. Their values are listed in table 5, together with the other parameters for diffusion creep. Using, these values the theoretical contribution of diffusion can be calculated and is shown in Figure 28.

Table 4. Constitutive

flow law parameters	A	unit	n	p	Q	unit	Reference
GBS T>255 K	3,00E+26	Mpa/m2/s	1,8	1,4	192	kJ/mol	Goldsby & Kohlstedt (2001)
Disl. creep T>262 K	6,96E+23	Mpa/s	4	0	155	kJ/mol	Paterson (1994)
Glen T>263 K	1,73E+21	Mpa/s	3	0	139	kJ/mol	Paterson (1994)

Table 5. Diffusion creep parameters

		Value	Unit	Reference
Burgers vector	b	4,52E-10	m	
Molar volume	Vm	1,97E-05	m3	
Gas constant	R	8,314	J/K/mol	
Preexponential volume diffusion	D0v	9,10E-04	m2/s	Ramseier (1967)
Activation energy for volume diffusion	Qv	59400	J/mol	Ramseier (1967)
Preexponential grain boundary diffusion	D0gb	8,40E-04	kJ/mol	Ramseier (1967)
Activation energy for grain boundary diffusion	Qgb	49000	J/mol	Goldsby & Kohlstedt (1997)
Grain boundary width (2b)	δ	9,04E-10	m	Frost and Ashby (1973)
Diffusivity of the fluid film at 273 K	Dfilm	2,50E-09	m2/s	Wang et al. (1953)

However, at temperatures above 258 K, an increase in grain boundary diffusion is expected due to the presence of the fluid film. The additional effect of this fluid film on grain boundary diffusion can be taken into account by replacing δ=2b with $\delta = w = 3.5(-T)^{1/2.4}$ in Equation 54 and by replacing D_{gb} with D_{film}. The liquid layer is of sufficient thickness to have the properties of bulk water and it can be expected that D_{film} is close to the value for the tracer coefficient of bulk water (diffusion of $H^1H^2O^{16}$ and $H^1H^3O^{16}$ in ordinary water) which is 2.5×10^9 at 273 K (Wang et al. 1953). No value for tracer diffusion in temperatures below 273 K have been determined, therefore a constant value for D_{film} is employed, resulting in an overestimation of fluid-film enhanced diffusion at lower temperatures (see Figure 28). The upper bound for fluid film enhanced diffusion is given by:

$$\dot{\epsilon} = \frac{42\sigma V_{\mathrm{m}}}{RTd^2}\Big(D_{\mathrm{v}} + \frac{w\pi}{d} D_{\mathrm{film}}\Big) \tag{55}$$

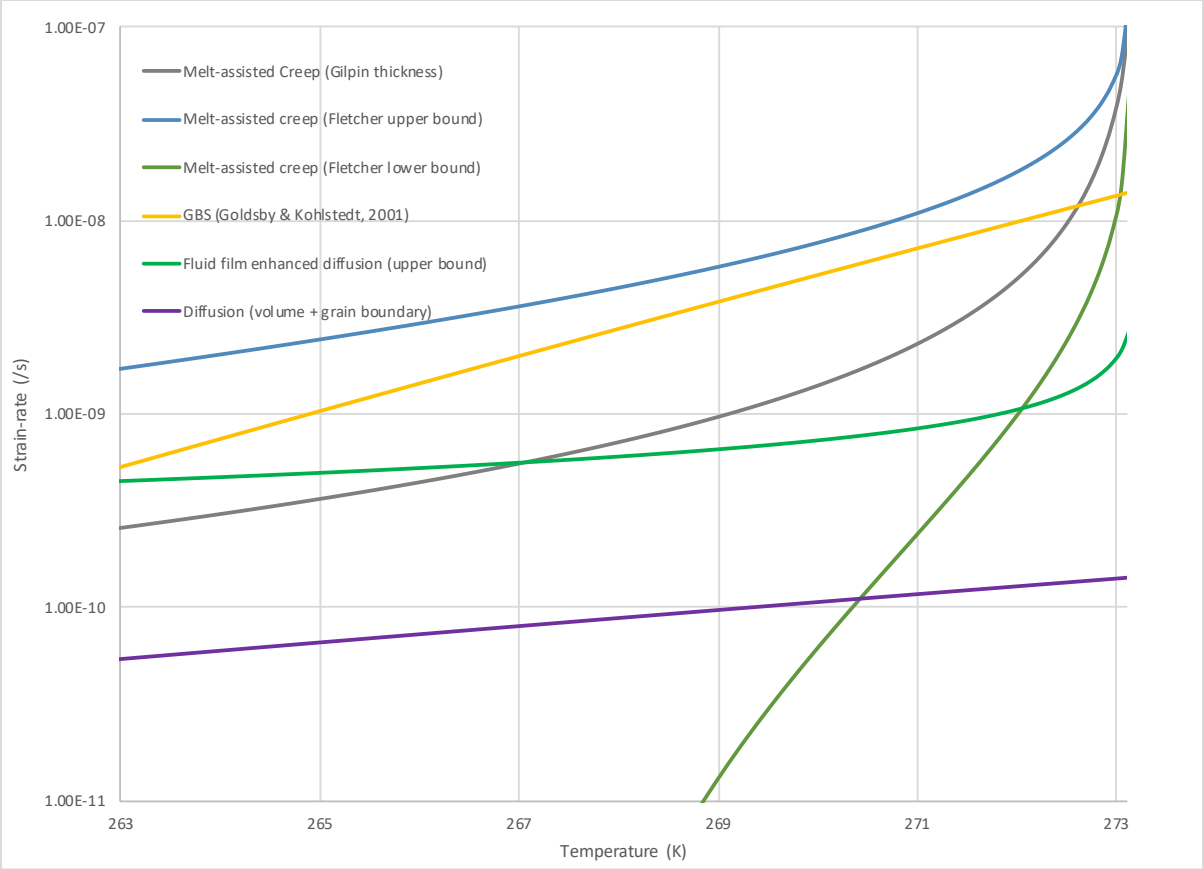

Figure 28: *A compilation of grain size sensitive mechanisms as a function of stress, at a constant stress of 0.1 MPa and a grain size of 1mm. Estimated rates for diffusion (Equation 54) and fluid film enhanced diffusion (Equation 55) are indicated by respectively the purple and light green line; GBS (Equation 53) is presented by the yellow line and Melt-assisted creep (Equation 39) is represented by: the dark green line (lower bound fluid film thickness of theoretical predictions by Fletcher (1968)), the blue line (upper bound fluid film thickness of theoretical predictions by Fletcher (1968)) and the grey line (fluid film thickness based on Gilpin (1980)).*

Figure 28 shows that the diffusional strain-rates are insignificant (1-2 orders of magnitude smaller) when compared to GBS. In addition, the model for Melt-assisted creep (Equation 39) can be added to this graph. Both the upper and lower bound of the theoretical predictions on fluid film thickness (Equation 19) and the inferred thickness of wire regalation (Equation 20) are used to get three different estimates for melt-assisted creep. Using the upper bound of Equation 19 as input for the fluid film thickness, predicts that for the complete range of temperatures showed in this figure (T>263 K) melt-assisted creep results in strain-rates which are higher as the GBS curve Goldsby and Kohlstedt (1997, 2001). At $\leq$268 K there is strong experimental evidence that deformation can be described by a stress-exponent of n=1.8 (e.g. Steinemann 1954; Glen 1955; Goldsby and Kohlstedt 1997, 2001) (see Figure 7 and table 3) and it is unlikely that melt-assisted creep is dominant at these temperatures. If it is assumed that the fluid film thickness can be described by Gilpin (1980) (Equation 20), then a transition to melt-assisted creep occurs at 272.65 K (-0.5°C) and the lower bound of Equation 19 predicts a transition at 273 K (-0,15°C). For all three solutions, the predicted strain-rates increase very rapidly (by one order of magnitude) when the temperature approaches the melting point.

5.2.2 Evidence for n=1 and p=3 in creep experiments at T>272 K

This rapid increase in strain-rates when the ice approaches the melting point has been observed in creep experiments on polycrystalline ice (e.g. Morgan 1991) (see Figure 9), which suggest that there is a switch in deformation mechanism around 272-273 K. If melt-assisted creep is responsible for the increase in strain-rates, then a stress-exponent of n=1 and a grain size exponent of p=3 should be observed in creep experiments at this temperature. Hence, strain-rates of creep experiments $\geq$272.6 K should be

described by the lines indicated in Figure 18 & 19. A stress exponent of n=1.3 has been observed in creep experiments at a constant temperature of 273.14 K and stress ranging from 0.01 - 0.1 MPa. Marshall et al. (2002) analyzed strain rates using borehol tilt measurements in temperate ice of the Worthington glacier and note n∼1 at low stress <1.8 kPa.

The experiments performed by Goldsby and Kohlstedt (1997, 2001) indicate a stress-exponent of n=1.8 and a grain size exponent of p=1.4, but they extrapolated their strain-rates to higher temperatures and did not perform experiments at T>268 K. Figure 7 shows a compilation of creep data close to the melting point and the solid curves indicate solutions of the composite flow law (Equation 17). However, the creep experiments in this graph of Glen (1955) are taken at temperatures below the expected transition temperature (T∼ 272.6 K) (triangles, 271 K) or at high stress (circles, >1 MPa). Colbeck and Evans (1973) found a better fit for their creep data using n=1.3. Goldsby and Kohlstedt (1997, 2001) estimated a grain size exponent of p=1.4, but as they did not perform experiments above 268 K a transition from p=1.4 to p=3 is possible, as none of the other creep experiments performed above 272 K (e.g. Glen 1955; Colbeck and Evans 1973) indicated, studied or published a dependency on grain size (also see table 3). The creep experiments showed in Figure 29 are all acquired at a grain size of ≥1 mm, which makes the data less reliable in studying GSS creep. Hence, a mechanism switch close to the melting point and a change in stress- and grain size exponent can not be excluded, but hard and consistent evidence, especially for a grain size exponent of p=3, is lacking.

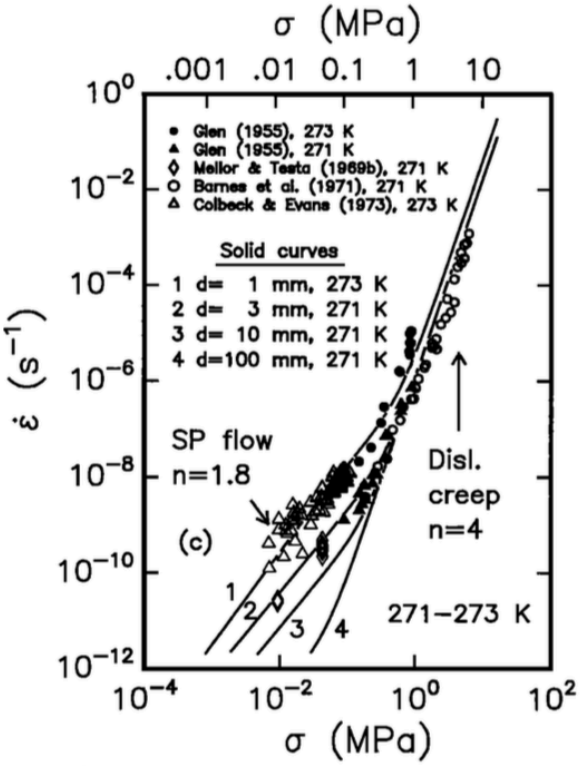

Figure 29: *Compilation of creep experiments at 271-273 K. Solid curves show the composite flow law (Equation 17) at different temperatures and grain sizes.*

5.2.3 Melt-assisted creep: a flow law for temperate ice?

The present theoretical model for polycrystalline ice predicts a switch from GBS to melt-assisted creep at T∼272.6 K in fine-grained ice (1mm) at low stress (0.1 MPa). At even lower stresses, this transition occurs at slightly lower temperatures, but at larger grain sizes (≥10 mm) there is no predicted switch to melt-assisted creep. Figure 28 shows that the contribution of diffusion can be neglected in the deformation of ice. Hence, the two existing flow laws for ice (Glen's flow law: Equation 8 and the composite flow law: Equation 17) can be used to show that melt-assisted creep becomes faster in ice close to the melting temperature (see Figure 30).

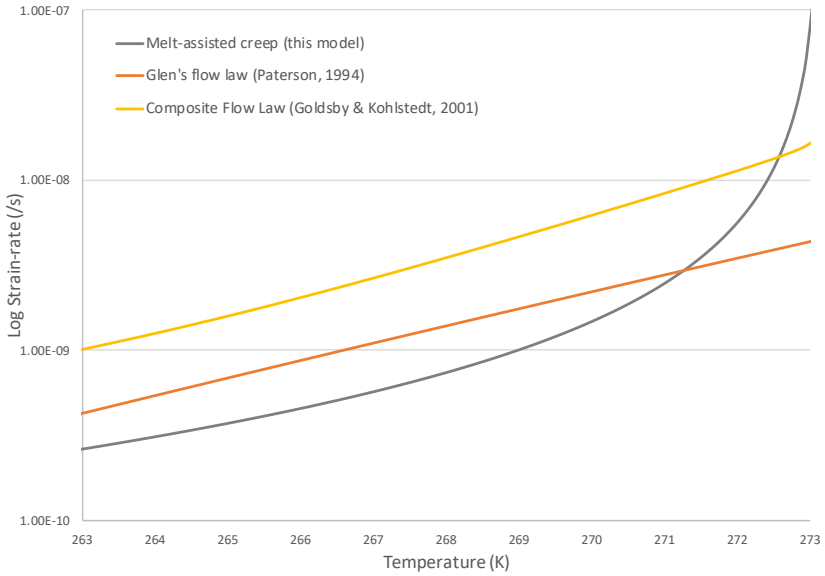

Figure 30: *Glen's flow law, the composite flow law and strain-rates derived in this study for melt-assisted creep as a function of temperature at constant stress (0.1 MPa) and for a grain size of 1 mm.*

At a grain size of 1 mm, the strain-rate predictions by the composite flow law prove to be more accurate than the conventional grain size independent flow law of Glen. Nevertheless, Figure **??** shows that melt-assisted creep enhances strain-rates by one order of magnitude. Therefore, this study suggest that the composite flow law requires modification to account for melt-assisted creep. This new composite flow law is then by given by:

$$\dot{\epsilon} = A_{\text{disl}}\sigma^4 * exp\Big(\frac{-Q_{\text{disl}}}{RT}\Big) + A_{\text{GBS}}\frac{\sigma^{1.8}}{d^{1.4}} * exp\Big(\frac{-Q_{\text{GBS}}}{RT}\Big) + A_{\text{mac}}\frac{\sigma^1}{d^3} * \Big(\frac{w^3(T)}{\eta_{\text{eff}}(T,w)}\Big) \tag{56}$$

in which A_{mac}=2,91 (see Equation 39). The contributions on strain-rates as a function of stress of each of the three constituents of this flow law (dislocation creep, GBS and melt-assisted creep) are plotted in Figure 31 (272 K, 1 mm), Figure 32 (273 K, 1 mm) and Figure 33 (273 K, 10 mm).

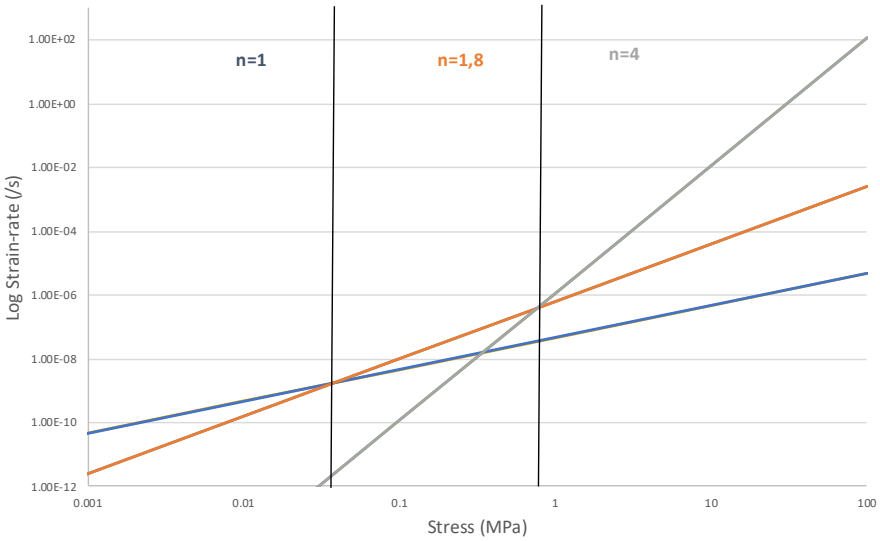

Figure 31: *The contribution of: (1) melt-assisted creep (blue), (2) Grain boundary sliding (orange) and (3) dislocation creep (grey) as a function of stress at 272 K for a grain size of 1 mm. Melt-assisted creep becomes dominant at σ <0.3 MPa.*

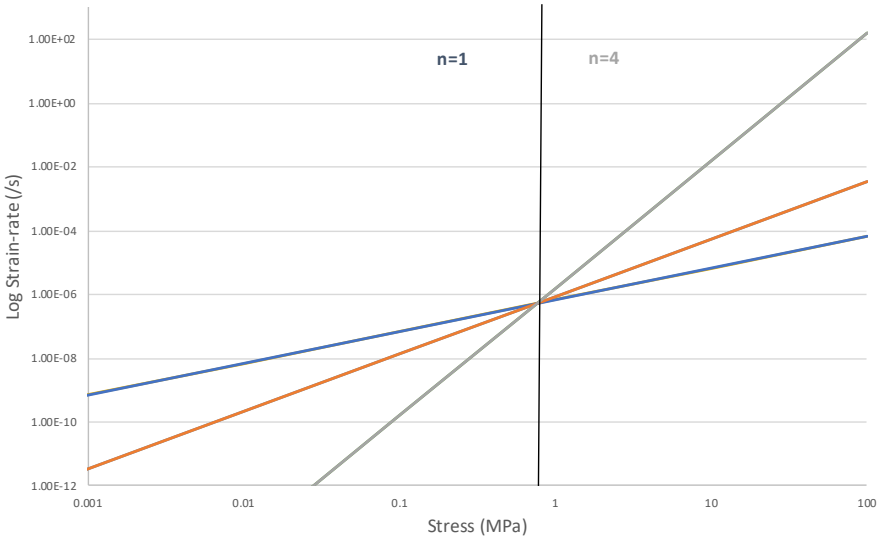

Figure 32: *The contribution of: (1) melt-assisted creep (blue), (2) Grain boundary sliding (orange) and (3) dislocation creep (grey) as a function of stress at 273 K for a grain size of 1 mm. Melt-assisted creep becomes dominant at σ <0.9 MPa. At higher stress, there is a direct transition to dislocation creep and no GBS regime is predicted.*

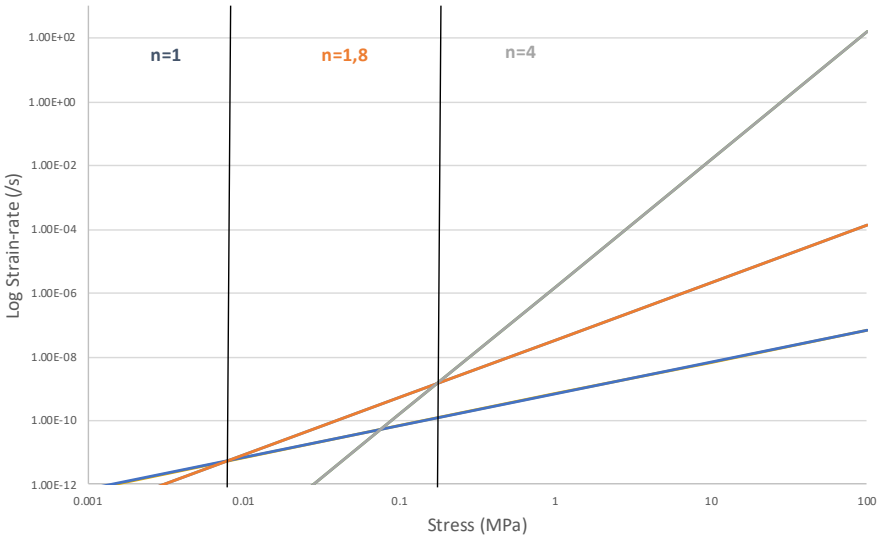

Figure 33: *The contribution of: (1) melt-assisted creep (blue), (2) Grain boundary sliding (orange) and (3) dislocation creep (grey) as a function of stress at 273 K for a grain size of 1 mm. Melt-assisted creep becomes dominant at σ <0.009 MPa.*

Figure 32 predicts that melt-assisted creep is dominant in temperate ice with a small grain size. As temperatures decrease (Figure 31 or as grain size starts to increase (Figure 33), GBS and dislocation creep become more important. Hence, the contribution of melt-assisted creep at stresses relevant for ice sheets (0.01-1 MPa) quickly diminishes at lower temperatures (T<271 K) and larger grain sizes (d>10mm).

5.3 Melt-assisted creep in ice sheets: implications

5.3.1 Presence of a temperate layer at the base of an ice sheet

Whether melt-assisted creep can take place in natural ice, in large part depends on the temperatures reached in ice sheets. The internal deformation of cold ice, up to $\sim$ 272 K (corrected for change in

pressure melting point), can be described reasonably accurate using Glen's flow law or the composite flow law. However, this flow law does not describe (warm) basal sliding of the ice sheet. At the base of an ice sheet heat production by frictional heating and geothermal heat flux can account for the presence of temperate ice (see Figure 34). A layer of temperate ice has no thermal gradient and therefore forms a near ideal thermal barrier (Aschwanden and Blatter 2005) which makes it difficult for such a layer to thicken. However, Krabbendam (2016) suggests that there are mechanisms that cause this layer to grow. Energy can be added to the temperate layer by: (1) bedrock highs elevated above the average height of the bedrock, conducting heat into the cold ice, (2) thickening by internal deformation due to folding and thrusting of heterogeneous ice flow near obstacles (e.g. Bell et al. 2014), (3) strain heating due to a difference in strain-rates in the temperate ice below the cold-temperate boundary (CTB) and cold ice above the CTB (Cuffey and Paterson 2010) and (4) upwards migration of water as a result of hydraulic fracturing or percolation (Krabbendam 2016). Although permeability in ice is small (Lliboutry 1971), even a small flux of water can transport a lot of heat, due to the large latent heat associated with the freezing of water. Freezing 1 kg of water heats up 160 kg of ice by 1 K (Paterson 1994). A combination of these processes can account for a significant layer of temperate ice at the base of an ice sheet.

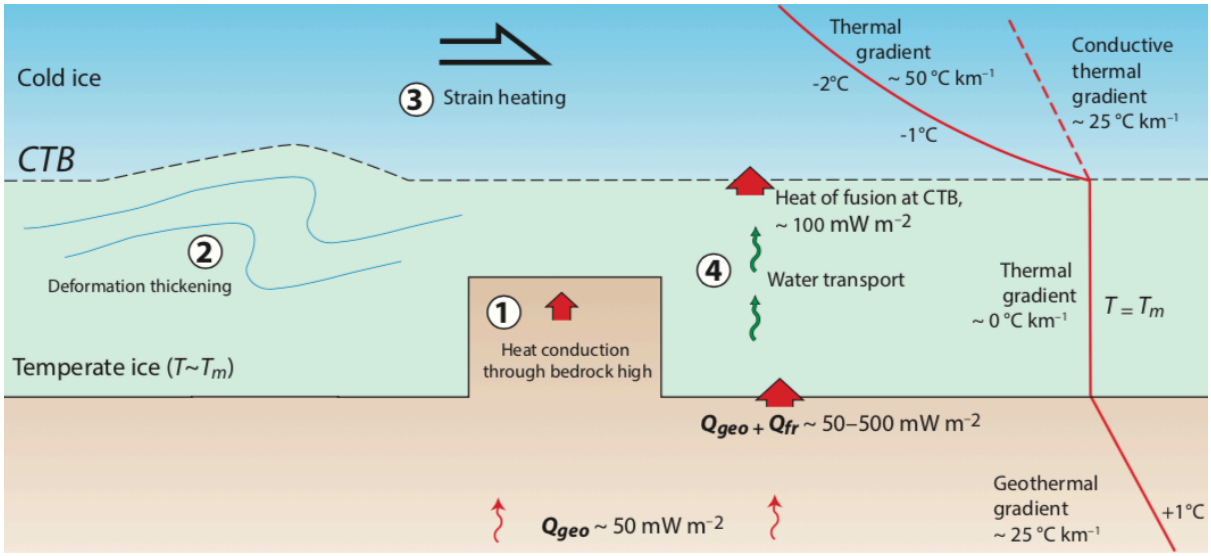

Figure 34: *Schematic drawing explaining the presence of a temperate layer at the base of an ice sheet from Krabbendam (2016). Thermal gradient based on the western Greenland ice core (Lüthi et al. 2002). Numbers 1-4 indicate processes that result in the formation and growth of the temperate layer. The basics of these processes are explained in the text.*

Evidence for the presence of temperate ice in ice sheets has been given by the lowermost 30m of a drilling core of the western Greenland ice sheet (Lüthi et al. 2002) and has also been modelled to occur beneath other parts of the Greenland ice sheet (Dahl-Jensen 1989; Calov and Hutter 1996; Greve 1997). To account for different rheological properties at the base of ice sheets, modern ice sheet models use an empirical drag factor or slip coefficient (e.g. MacAyeal et al. 1995; Gudmundsson and Raymond 2008). The necessary low drag at their base requires the presence of soft sediment or deformable till (e.g. Alley et al. 1986; Hindmarsh 1997; Winsborrow et al. 2010). However, there is evidence for fast ice flow on hard, rough bedrock implying other mechanisms must be operating in the basal part of the ice sheet that explain the fast flow (e.g. Kleman et al. 2008; Rippin 2013; Krabbendam et al. 2016). This study provides a possible theoretical explanation for an increase in strain-rates when the ice is close or at the melting temperature.

If the grain size of this basal layer appears to be small ($\leq$1 mm), a transition from a regime that can be modelled using Glen's flow law or the composite flow law above the CTB to a melt-assisted creep regime below the CTB may occur in regions of ice sheets where friction with the bed-rock is high, such as ice-streams on hard beds. A layer of 30m is relatively thin compared to the total thickness of the ice sheet (~2500m), but if strain-rates in this layer are one order of magnitude larger, then a substantial percentage of the observed velocities at the surface of ice-streams is controlled by flow in this

basal temperate layer. This could explain the fast flow rates observed in the Jakobshavn Isbræ (Lüthi et al. 2002), which is observed to contain a temperate layer, and possibly the Northeast Greenland ice stream (NEGIS) (Krabbendam 2016). A large part of Greenland is dominated by Precambrian gneisses and it is expected that much of the ice sheet is underlain by such rocks. These rocks are very hard to deform and generate a lot of friction (and heat). Hence, it is likely that large parts of the Greenland ice-streams are sliding on these rocks and a temperate basal layer may exist. Thus, melt-assisted creep may play a role in the rheology of ice-streams. A large part of the area covered by the Laurentide ice sheet and the Eurasian ice sheet during the last ice age is also dominated by Precambrian gneisses (Canada, Scotland and Scandinavia), therefore melt-assisted creep may also have played a role in the dynamics of ice sheets in the past.

5.3.2 Dynamic recrystallization and grain growth in ice sheets

The contribution of melt-assisted creep on deformation becomes very small at large grain sizes >>1 mm. However, there are several ice cores (e.g. Gow and Williamson 1976; Woods 1994; Eichler et al. 2013; Thorsteinn Thorsteinsson et al. 1997) (see Figure 35a) that show a sudden increase in grain size in the bottom part of multiple ice cores, where temperatures are reached that favour melt-assisted creep. Eichler et al. (2013) found grains with a cross sectional area of up to 10^3 mm^2 (diameters of up to 40 mm) (see Figure 5) in the NEEM ice core. Very large grains with a cross-sectional area of up to 30 cm^2 have been retrieved from the core at Byrd station in West Antarctica (Gow and Williamson 1976). This increase in grain sizes is associated with grain growth as result of migration recrystallization (Woods 1994; Duval et al. 1983). Migration recrystallization involves migration of the grain boundary and is driven by a difference in internal (Helmholtz) energy between two grains. A grain with a low energy consumes a grain with high energy, thereby leading to grain growth. The velocity at which the grain boundary moves depends on the mobility of the grain boundary and the difference in Helmholtz energy. The mobility of the grain boundary is expected to be enhanced by the presence of a fluid (Peach et al. 2001). Migration recrystallization is observed in ice above 263 K (Duval et al. 1983). High temperatures allow the nucleation of new grains and the pre-melted films on the grain boundary are expected to enhance the mobility of the grain boundaries close to the melting point. Below 263 K dynamic recrystallization is expected to occur, but the grain boundary mobility is lower and rotation recrystallization is dominant, which is not associated with grain growth of such high rates.

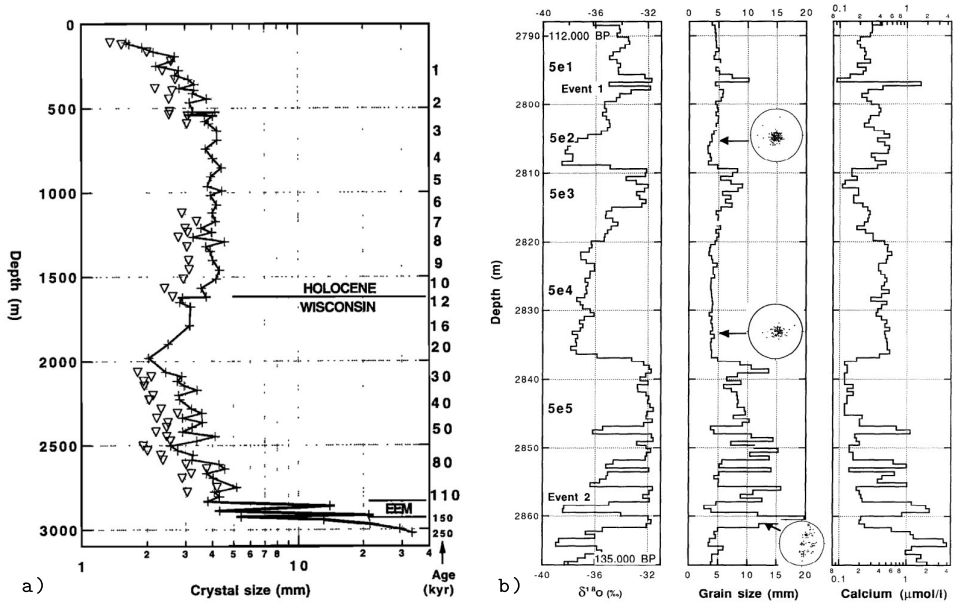

Figure 35: *Grain size with depth for the GRIP ice core (Thorsteinn Thorsteinsson et al. 1995; Thorsteinn Thorsteinsson et al. 1997). A clear increase in grain size is observed below 2800m depth. (a) Grain size data measured with linear intercept method for GRIP ice core and (b) GRIP ice core in between 2790m and 2870m, showing a correlation of grain size with soluble calcium (Ca^{2+}). Data from the Eemian show a close correlation between Ca^{2+} and dust content (Thorsteinn Thorsteinsson et al. 1997). Hence, calcium is believed to be a good indicator for impurity content.*

The widespread observed increase in grain size at the bottom of ice sheets may suggest that migration recrystallization is far more important than melt-assisted creep in the deformation of temperate ice. However, Alley and Woods (1996) and Thorsteinn Thorsteinsson et al. (1995) show that very often an alternation between very coarse and finer grained layers is observed in the basal part of ice sheets. This alternation can be correlated to the impurity content (see Figure 35b). Layers with a high impurity content are characterized by a small grain size. Woods (1994) also show that very close to the bedrock the grain size decreases again, due to mixing with silt from the underlying bedrock. Gow and Williamson (1976) show that layers with volcanic dust contain very fine grained ice. Therefore, it is expected that in these layers the impurity content inhibits grain growth and the mechanism proposed in this study may be dominant. A complicating factor to attribute deformation in these layers to melt-assisted creep is that a strong single maximum CPO is observed. CPO in general is linked to be the result of dislocation creep at relatively high strain-rates: a combination of grain rotation and preferred slip on the basal plane, result in ice in which the c-axes are aligned (see Figure 4 & 6). The accommodating mechanism of GBS is basal slip and hence it is expected that just as in dislocation creep, GBS (e.g. Goldsby and Kohlstedt 2001) is also accompanied by the formation of a CPO. It is generally accepted that diffusion creep is not accompanied with the formation of a CPO as it has the same rates in any direction and does not depend on the orientation of the crystallographic planes. Although transport in this model is governed by viscous flow instead of diffusion it is expected that like diffusion it does not produce a CPO. However, there has been evidence for formation of a CPO by interface controlled diffusion in olivine and orthopyroxene (Sundberg and Cooper 2008) and diffusion in olivine when a melt phase is present (Miyazaki et al. 2013), due to orientation of crystallographic planes on grain boundaries. If the kinetics of the formation of the pre-melted liquid layer or the freezing kinetics are faster in certain crystallographic directions, then the mechanism proposed in this thesis may result in the formation of a CPO.

Migration recrystallization is dominant in ice above 263 K, but in general it is expected that a combination of rotation and migration recrystallization takes place (Drury and Urai 1990). Recrystallization is not only associated with grain growth but also with grain size reduction, due to the nucleation of new grains by progressive rotation of subgrains and nucleation by local bulges formed by grain boundary migration. Hence, the grain size is expected to be related to a balance between grain growth and grain size reduction, which is given by: $D^4 \approx \frac{V_{GB}}{R_N}$ in which D is the recrystallized grain size, V_{GB} is the grain boundary velocity and R_N is the rate of nuclei formed per second. The large grain size in these basal layers suggest that V_{GB} becomes very fast in these temperate layers. At the same time it has been observed that the size of the recrystallized grains can be related to the steady state flow stress when materials (including metals, rocks and ceramics) are deformed at constant strain-rate. Experiments show that this D-σ relation can be expressed by:

$$D = K\sigma^m \tag{57}$$

in which K and m are material and mechanism specific constants (Twiss 1977). Jacka and Jun (1994) show that for ice an m-value of 0.85 can be obtained. De Bresser et al. (2001) hypothesize that the recrystallized grain size (Equation 57) in olivine and calcite tends to organize itself on the boundary between GSS and GSI creep. Whether recrystallized grain size in ice also may represent a boundary between GSS and GSI creep is difficult to say. The very large (recrystallized) grain size in the coarse grained layers of temperate ice suggest that (GSS) dislocation creep is dominant. However, the nucleated grains are initially small and GSS creep may initially play a role until the grains reach a size in which GSI creep (dislocation creep) becomes dominant (De Bresser et al. 2001). Hence, it may very well be that melt-assisted creep plays a role in deformation of these grains until grain growth becomes more important.

Although temperatures in the basal part of the ice sheet favor melt-assisted creep, the increase in grain size suggest that grain growth by migration recrystallization becomes very fast under these conditions. This prevents melt-assisted creep to be the dominant mechanism in temperate ice. If grain growth is inhibited, as is expected for layers with a high impurity content, then melt-assisted can become the dominant mechanism and strain-rates may be described by the model derived in this study. However, it remains questionable whether this can be reconciled with the observed formation of a strong CPO in these layers.

5.4 Recommendations for future work

When performing wire regalation experiments, the apparatus should be designed in such a way that the sample can equilibrate before the load is applied. The setup needs to be designed in such a way that a constant temperature can be maintained, without any temperature gradients between the cooling tank and the sample container. A possible way to achieve this is by changing the design of the apparatus, such that the sample is at the bottom of the apparatus and the weights can be applied at the top. To assess whether melt-assisted creep by grain boundary viscous flow takes place in polycrystalline ice requires creep experiments on fine grained ice very close to the melting temperature. This is necessary to determine if there is a change in stress and grain size exponent close to the melting point. Creep experiments of Goldsby and Kohlstedt (1997, 2001) have been performed only up to T$\sim$268 K and other creep experiments under these conditions have been performed on grain sizes, which are too large to determine GSS mechanisms. If a change to a linear stress-exponent is observed in experiments, it is relevant to test the difference in strain-rates predicted by the composite flow law derived in this thesis (Equation 56) with Glen's flow law and the composite flow law of Goldsby and Kohlstedt (2001). The appearance of very large grains in the basal part of the ice sheets is attributed to an increase in migration recrystallization at higher temperatures. This may for a very large part be the result of the fluid films, as it is expected that these fluid films increase the grain boundary mobility. This effect is described qualitatively, but a similar theory as derived in this thesis may be used to quantitatively describe the grain growth as a function of fluid film thickness.

6 Conclusion

Based on an analysis of the theoretical models for melt-assisted creep and an evaluation of this mechanism on creep in ice, the following conclusions can be drawn:

- The thickness of the pre-melted fluid films is sufficient to sustain viscous flow down to at least 268 K, which would favor grain boundary transport by viscous flow which results in faster transport rates than diffusion.
- The model for melt-assisted creep in polycrystalline ice derived in this study is characterized by a stress-exponent of n=1 and a grain-size exponent of p=3.
- It is difficult to obtain convincing data from creep experiments in polycrystalline ice close to the melting point that substantiate the stress- and grain-size exponent predicted by this model. However, experimental data on wire regalation confirms that the velocity of the wire is linearly related to stress and inverse cubic dependent on wire diameter and it is expected that melt-assisted creep in polycrystalline ice is controlled by the same kinetics.
- The model for polycrystalline ice predicts that a transition from GBS to melt-assisted creep occurs just below the melting point. At a stress of 0.1 MPa and a grain-size of 1 mm, this occurs around 272.6 K. At the melting temperature, melt-assisted creep predicts an increase in strain-rates by one order of magnitude.
- Grain boundary melt transport may play a role in the rheology of ice sheets. At the base of ice sheets temperate layers are formed in which temperatures are reached that favor our model for melt-assisted creep.
- The large grain size at the bottom of ice sheets suggest that grain growth prevents melt-assisted creep to be the dominant deformation mechanism. In layers with a high impurity content grain growth is inhibited, for these layers melt-assisted creep may play an important role and become the dominant deformation mechanism based on the theory presented in this thesis. Conventional flow laws for ice rheology do not consider this effect and may underestimate strain-rates in these layers. However, in these layers a strong CPO is observed and it remains questionable whether this can be reconciled with flow by grain boundary melt transport as dominant deformation mechanism.

7 Acknowledgments

I would like to express my gratitude towards Prof. Dr. Chris Spiers, who has been a very inspiring supervisor and motivated me to go the extra mile and continue despite difficulties. During the past year I have learned an extensive amount, not just about ice rheology. I also would like to thank my colleagues at the High Pressure Temperature lab for their help and interest, especially the other Master students with whom I shared a room for the past year. Last but not least I would like to thank the technical staff for their assistance in a hectic period where the lab was moving to a new building.

8 References

References

Alley, Richard B, Donald D Blankenship, Charles R Bentley, and ST Rooney. 1986. "Deformation of till beneath ice stream B, West Antarctica." *Nature* 322 (6074): 57.

Alley, Richard B, Peter U Clark, Philippe Huybrechts, and Ian Joughin. 2005. "Ice-sheet and sea-level changes." *science* 310 (5747): 456–460.

Alley, Richard B, and GA Woods. 1996. "Impurity influence on normal grain growth in the GISP2 ice core, Greenland." *Journal of Glaciology* 42 (141): 255–260.

Aschwanden, Andy, and Heinz Blatter. 2005. "Meltwater production due to strain heating in Storglaciären, Sweden." *Journal of Geophysical Research: Earth Surface* 110 (F4).

Ashby, MF, and RA Verrall. 1973. "Diffusion-accommodated flow and superplasticity." *Acta metallurgica* 21 (2): 149–163.

Barnes, P, and D Tabor. 1969. "Plastic flow and pressure melting in the deformation of ice." PhD diss., University of Cambridge.

Batchelor, Cx K. 1967. *An introduction to fluid dynamics.* Cambridge university press.

Bell, Robin E, Kirsteen Tinto, Indrani Das, Michael Wolovick, Winnie Chu, Timothy T Creyts, Nicholas Frearson, Abdulhakim Abdi, and John D Paden. 2014. "Deformation, warming and softening of Greenland's ice by refreezing meltwater." *Nature Geoscience* 7 (7): 497.

Bintanja, R, and RSW Van de Wal. 2008. "North American ice-sheet dynamics and the onset of 100,000-year glacial cycles." *Nature* 454 (7206): 869.

Budd, WF, and TH Jacka. 1989. "A review of ice rheology for ice sheet modelling." *Cold Regions Science and Technology* 16 (2): 107–144.

Byers, John, Denis Cohen, and Neal R Iverson. 2012. "Subglacial clast/bed contact forces." *Journal of Glaciology* 58 (207): 89–98.

Calov, Reinhard, and Kolumban Hutter. 1996. "The thermomechanical response of the Greenland ice sheet to various climate scenarios." *Climate Dynamics* 12 (4): 243–260.

Chan, Derek YC, and RG Horn. 1985. "The drainage of thin liquid films between solid surfaces." *The Journal of chemical physics* 83 (10): 5311–5324.

Church, John A, J Stuart Godfrey, David R Jackett, and Trevor J McDougall. 1991. "A model of sea level rise caused by ocean thermal expansion." *Journal of Climate* 4 (4): 438–456.

Colbeck, Samuel C, and RJ Evans. 1973. "A flow law for temperate glacier ice." *Journal of Glaciology* 12 (64): 71–86.

Cuffey, Kurt M, and William Stanley Bryce Paterson. 2010. *The physics of glaciers.* Academic Press.

Dahl-Jensen, Dorthe. 1989. "Steady thermomechanical flow along two-dimensional flow lines in large grounded ice sheets." *Journal of Geophysical Research: Solid Earth* 94 (B8): 10355–10362.

Dash, JG, AW Rempel, and JS Wettlaufer. 2006. "The physics of premelted ice and its geophysical consequences." *Reviews of modern physics* 78 (3): 695.

De Bresser, J, J Ter Heege, and C Spiers. 2001. "Grain size reduction by dynamic recrystallization: can it result in major rheological weakening?" *International Journal of Earth Sciences* 90 (1): 28–45.

Drake, LD, and RL Shreve. 1973. "Pressure melting and regelation of ice by round wires." *Proceedings of the Royal Society of London. A. Mathematical and Physical Sciences* 332 (1588): 51–83.

Driesschaert, Emmanuelle, Thierry Fichefet, Hugues Goosse, Philippe Huybrechts, I Janssens, Anne Mouchet, Guy Munhoven, Victor Brovkin, and SL Weber. 2007. "Modeling the influence of Greenland ice sheet melting on the Atlantic meridional overturning circulation during the next millennia." *Geophysical Research Letters* 34 (10).

Drury, Martyn R, and Janos L Urai. 1990. "Deformation-related recrystallization processes." *Tectonophysics* 172 (3-4): 235–253.

Duval, P. 1977. "The role of the water content on the creep rate of polycrystalline ice." *IAHS Publ* 118:29–33.

Duval, P, and M Montagnat. 2002. "Comment on "Superplastic deformation of ice: Experimental observations" by DL Goldsby and DL Kohlstedt." *Journal of Geophysical Research: Solid Earth* 107 (B4): ECV–4.

Duval, Paul, MF Ashby, and I Anderman. 1983. "Rate-controlling processes in the creep of polycrystalline ice." *The Journal of Physical Chemistry* 87 (21): 4066–4074.

Eichler, J, Ina Kleitz, Maddalena Bayer-Giraldi, Daniela Jansen, Sepp Kipfstuhl, Wataru Shigeyama, Christian Weikusat, and Ilka Weikusat. 2017. "Location and distribution of micro-inclusions in the EDML and NEEM ice cores using optical microscopy and in situ Raman spectroscopy." *The Cryosphere* 11 (3): 1075–1090.

Eichler, J, I Weikusat, and S Kipfstuhl. 2013. "Orientation-tensor eigenvalues along the NEEM ice core." *PANGAEA.*

Elbaum, Michael, and M Schick. 1991. "Application of the theory of dispersion forces to the surface melting of ice." *Physical review letters* 66 (13): 1713.

Ewert, H, A Groh, and R Dietrich. 2012. "Volume and mass changes of the Greenland ice sheet inferred from ICESat and GRACE." *Journal of Geodynamics* 59:111–123.

Faraday, M. 1850. "M. Faraday, The Athenaeum 1181, 640 (1850)." *The Athenaeum* 1181:640.

Faria, Sérgio H, Ilka Weikusat, and Nobuhiko Azuma. 2014a. "The microstructure of polar ice. Part I: Highlights from ice core research." *Journal of Structural Geology* 61:2–20.

———. 2014b. "The microstructure of polar ice. Part II: State of the art." *Journal of Structural Geology* 61:21–49.

Faria, SH, and K Hutter. 2001. "The challenge of polycrystalline ice dynamics." *Advances in Thermal Engineering and Sciences for Cold Regions:* 3–31.

Fletcher, NH. 1968. "Surface structure of water and ice: II. A revised model." *Philosophical Magazine* 18 (156): 1287–1300.

———. 1973. "The surface of ice." *Physics and chemistry of ice:* 132–136.

García Fernandez, Ramon, José LF Abascal, and Carlos Vega. 2006. "The melting point of ice I h for common water models calculated from direct coexistence of the solid-liquid interface." *The Journal of chemical physics* 124 (14): 144506.

Gilpin, RR. 1979. "A model of the "liquid-like" layer between ice and a substrate with applications to wire regelation and particle migration." *Journal of colloid and interface science* 68 (2): 235–251.

———. 1980. "Wire regelation at low temperatures." *Journal of Colloid and Interface Science* 77 (2): 435–448.

Glen, John W. 1955. "The creep of polycrystalline ice." *Proc. R. Soc. Lond. A* 228 (1175): 519–538.

Goldsby, DL, and DL Kohlstedt. 1997. "Grain boundary sliding in fine-grained ice I." *Scripta Materialia* 37 (9): 1399–1406.

Goldsby, DL, and DL Kohlstedt. 2001. "Superplastic deformation of ice: Experimental observations." *Journal of Geophysical Research: Solid Earth* 106 (B6): 11017–11030.

Gow, Anthony J, and Terrence Williamson. 1976. "Rheological implications of the internal structure and crystal fabrics of the West Antarctic ice sheet as revealed by deep core drilling at Byrd Station." *Geological Society of America Bulletin* 87 (12): 1665–1677.

Greve, Ralf. 1997. "Application of a polythermal three-dimensional ice sheet model to the Greenland ice sheet: response to steady-state and transient climate scenarios." *Journal of Climate* 10 (5): 901–918.

Gudmundsson, G Hilmar, and Melanie Raymond. 2008. "On the limit to resolution and information on basal properties obtainable from surface data on ice streams." *The Cryosphere Discussions* 2 (3): 413–445.

Hall, Donald L, S Michael Sterner, and Robert J Bodnar. 1988. "Freezing point depression of NaCl-KCl-H 2 O solutions." *Economic Geology* 83 (1): 197–202.

Hindmarsh, Richard. 1997. "Deforming beds: viscous and plastic scales of deformation." *Quaternary Science Reviews* 16 (9): 1039–1056.

Hondoh, Takeo. 2000. *Physics of ice core records.* Sapporo: Hokkaido univ. press.

Israelachvili, Jacob N. 1986. "Measurement of the viscosity of liquids in very thin films." *Journal of colloid and interface science* 110 (1): 263–271.

Ivins, Erik R, Thomas S James, John Wahr, Ernst J O. Schrama, Felix W Landerer, and Karen M Simon. 2013. "Antarctic contribution to sea level rise observed by GRACE with improved GIA correction." *Journal of Geophysical Research: Solid Earth* 118 (6): 3126–3141.

Jacka, TH, and Li Jun. 1994. "The steady-state crystal size of deforming ice." *Annals of Glaciology* 20:13–18.

Jacka, Tim H, Shavawn Donoghue, Jun Li, William F Budd, and Ross M Anderson. 2003. "Laboratory studies of the flow rates of debris-laden ice." *Annals of Glaciology* 37:108–112.

Joly, J. 1887. "The phenomena of skating and Professor J. Tomson's thermodynamic relation." *Scientific Proceeding of the Royal Dublin Society, New Series* 5:453–454.

Joughin, Ian, Ben E Smith, Ian M Howat, Ted Scambos, and Twila Moon. 2010. "Greenland flow variability from ice-sheet-wide velocity mapping." *Journal of Glaciology* 56 (197): 415–430.

Kleman, Johan, Arjen P Stroeven, and Jan Lundqvist. 2008. "Patterns of Quaternary ice sheet erosion and deposition in Fennoscandia and a theoretical framework for explanation." *Geomorphology* 97 (1-2): 73–90.

Krabbendam, Maarten. 2016. "Sliding of temperate basal ice on a rough, hard bed: creep mechanisms, pressure melting, and implications for ice streaming." *The Cryosphere* 10 (5): 1915–1932.

Krabbendam, Maarten, Nick Eyles, Niko Putkinen, Tom Bradwell, and Lina Arbelaez-Moreno. 2016. "Streamlined hard beds formed by palaeo-ice streams: a review." *Sedimentary Geology* 338:24–50.

Kuhn, W, and M Thürkauf. 1958. "Isotopentrennung beim Gefrieren von Wasser und Diffusionskonstanten von D und 18O im Eis. Mit Diskussion der Möglichkeit einer Multiplikation der beim Gefrieren auftretenden Isotopentrennung in einer Haarnadelgegenstromvorrichtung." *Helvetica Chimica Acta* 41 (4): 938–971.

Kuiper, EN. 2019. "Flow in naturally deformed ice: a cryogenic electron microscopy and modelling study of the NEEM ice core." PhD diss., University Utrecht.

Kuroda, T, and R Lacmann. 1982. "Growth kinetics of ice from the vapour phase and its growth forms." *Journal of Crystal Growth* 56 (1): 189–205.

Langdon, TG. 1994. "A unified approach to grain boundary sliding in creep and superplasticity." *Acta Metallurgica et Materialia* 42 (7): 2437–2443.

Lliboutry, L. 1971. "Permeability, brine content and temperature of temperate ice." *Journal of Glaciology* 10 (58): 15–29.

Lüthi, Martin, Martin Funk, Almut Iken, Shivaprasad Gogineni, and Martin Truffer. 2002. "Mechanisms of fast flow in Jakobshavn Isbræ, West Greenland: Part III. Measurements of ice deformation, temperature and cross-borehole conductivity in boreholes to the bedrock." *Journal of Glaciology* 48 (162): 369–385.

MacAyeal, Douglas R, Robert A Bindschadler, and Theodore A Scambos. 1995. "Basal friction of ice stream E, West Antarctica." *Journal of Glaciology* 41 (138): 247–262.

Marshall, Shawn J. 2005. "Recent advances in understanding ice sheet dynamics." *Earth and Planetary Science Letters* 240 (2): 191–204.

Marshall, Shawn J, Thomas S James, and Garry KC Clarke. 2002. "North American ice sheet reconstructions at the Last Glacial Maximum." *Quaternary Science Reviews* 21 (1-3): 175–192.

Mellor, Malcolm, and Richard Testa. 1969. "Effect of temperature on the creep of ice." *Journal of Glaciology* 8 (52): 131–145.

Miyazaki, Tomonori, Kenta Sueyoshi, and Takehiko Hiraga. 2013. "Olivine crystals align during diffusion creep of Earth's upper mantle." *Nature* 502 (7471): 321.

Montagnat, Maurine, and Paul Duval. 2000. "Rate controlling processes in the creep of polar ice, influence of grain boundary migration associated with recrystallization." *Earth and Planetary Science Letters* 183 (1-2): 179–186.

Morgan, VI. 1991. "High-temperature ice creep tests." *Cold regions science and technology* 19 (3): 295–300.

Nye, JF, and FC Frank. 1973. "Hydrology of the intergranular veins in a temperate glacier." In *Symposium on the Hydrology of Glaciers,* 95:157–161. Citeseer.

Padmanabhan, Kuppuswamy Anantha, and Graeme J Davies. 1980. *Superplasticity.* Springer.

Paterson, WSB. 1994. *The physics of glaciers, 480 pp.*

Peach, CJ, CJ Spiers, and PW Trimby. 2001. "Effect of confining pressure on dilatation, recrystallization, and flow of rock salt at 150 C." *Journal of Geophysical Research: Solid Earth* 106 (B7): 13315–13328.

Peltier, WR. 1998. "Postglacial variations in the level of the sea: Implications for climate dynamics and solid-earth geophysics." *Reviews of geophysics* 36 (4): 603–689.

Pérez-Prado, Maria Teresa, MC Cristina, Oscar Antonio Ruano, and Gaspar González-Doncel. 1998. "Grain boundary sliding and crystallographic slip during superplasticity of Al–5% Ca–5% Zn as studied by texture analysis." *Materials Science and Engineering: A* 244 (2): 216–223.

Pluymakers, Anne MH, and Christopher J Spiers. 2015. "Compaction creep of simulated anhydrite fault gouge by pressure solution: theory v. experiments and implications for fault sealing." *Geological Society, London, Special Publications* 409 (1): 107–124.

Ramseier, Rene O. 1967. "Self-diffusion of tritium in natural and synthetic ice monocrystals." *Journal of Applied Physics* 38 (6): 2553–2556.

Reeh, Niels, Erik Lintz Christensen, Christoph Mayer, and Ole B Olesen. 2003. "Tidal bending of glaciers: a linear viscoelastic approach." *Annals of Glaciology* 37:83–89.

Rignot, E, J Mouginot, and B Scheuchl. 2011. "Ice flow of the Antarctic ice sheet." *Science* 333 (6048): 1427–1430.

Rippin, David M. 2013. "Bed roughness beneath the Greenland ice sheet." *Journal of Glaciology* 59 (216): 724–732.

Rothrock, Drew A, Yanling Yu, and Gary A Maykut. 1999. "Thinning of the Arctic sea-ice cover." *Geophysical Research Letters* 26 (23): 3469–3472.

Rutter, EH. 1976. "A Discussion on natural strain and geological structure-The kinetics of rock deformation by pressure solution." *Phil. Trans. R. Soc. Lond. A* 283 (1312): 203–219.

Sasgen, Ingo, Michiel van den Broeke, Jonathan L Bamber, Eric Rignot, Louise Sandberg Sørensen, Bert Wouters, Zdeněk Martinec, Isabella Velicogna, and Sebastian B Simonsen. 2012. "Timing and origin of recent regional ice-mass loss in Greenland." *Earth and Planetary Science Letters* 333:293–303.

Schulson, Erland M, and Paul Duval. 2009a. *Creep and fracture of ice.* Cambridge University Press.

———. 2009b. *Creep and fracture of ice.* Cambridge University Press.

Spiers, Christopher J, and Peter MTM Schutjens. 1990. "Densification of crystalline aggregates by fluid-phase diffusional creep." In *Deformation processes in minerals, ceramics and rocks,* 334–353. Springer.

Steinemann, Samuel. 1954. "Results of preliminary experiments on the plasticity of ice crystals." *Journal of Glaciology* 2 (16): 404–416.

Stern, Laura A, William B Durham, and Stephen H Kirby. 1997. "Grain-size-induced weakening of H2O ices I and II and associated anisotropic recrystallization." *Journal of Geophysical Research: Solid Earth* 102 (B3): 5313–5325.

Stocker, T, D Qin, Plattner, and A G Nauels. 2014. *Climate change 2013: the physical science basis: Working Group I contribution to the Fifth assessment report of the Intergovernmental Panel on Climate Change.* Cambridge University Press.

Stroeve, Julienne, Marika M Holland, Walt Meier, Ted Scambos, and Mark Serreze. 2007. "Arctic sea ice decline: Faster than forecast." *Geophysical research letters* 34 (9).

Sundberg, Marshall, and Reid F Cooper. 2008. "Crystallographic preferred orientation produced by diffusional creep of harzburgite: Effects of chemical interactions among phases during plastic flow." *Journal of Geophysical Research: Solid Earth* 113 (B12).

Telford, JW, and JS Turner. 1963. "The motion of a wire through ice." *Philosophical Magazine* 8 (87): 527–531.

Thomas, R, E Frederick, J Li, W Krabill, S Manizade, J Paden, J Sonntag, R Swift, and J Yungel. 2011. "Accelerating ice loss from the fastest Greenland and Antarctic glaciers." *Geophysical Research Letters* 38 (10).

Thomson, W. 1861. "Thomson, W., 1861, Proc. R. Soc. London 11, 198." *Proc. R. Soc. London* 11:198.

Thorsteinsson, Thorsteinn, Josef Kipfstuhl, Hajo Eicken, Sigfus J Johnsen, and Katrin Fuhrer. 1995. "Crystal size variations in Eemian-age ice from the GRIP ice core, central Greenland." *Earth and Planetary Science Letters* 131 (3-4): 381–394.

Thorsteinsson, Thorsteinn, Josef Kipfstuhl, and Heinz Miller. 1997. "Textures and fabrics in the GRIP ice core." *Journal of Geophysical Research: Oceans* 102 (C12): 26583–26599.

Thorsteinsson, Throstur, ED Waddington, KC Taylor, RB Alley, and DD Blankenship. 1999. "Strain-rate enhancement at Dye 3, Greenland." *Journal of Glaciology* 45 (150): 338–345.

Twiss, Robert J. 1977. "Theory and applicability of a recrystallized grain size paleopiezometer." In *Stress in the Earth,* 227–244. Springer.

Wang, Jui Hsin, Charles V Robinson, and IS Edelman. 1953. "Self-diffusion and structure of liquid water. III. Measurement of the self-diffusion of liquid water with H2, H3 and O18 as Tracers1." *Journal of the American Chemical Society* 75 (2): 466–470.

Weertman, J. 1955. "Theory of steady-state creep based on dislocation climb." *Journal of Applied Physics* 26 (10): 1213–1217.

Winsborrow, Monica CM, Chris D Clark, and Chris R Stokes. 2010. "What controls the location of ice streams?" *Earth-Science Reviews* 103 (1-2): 45–59.

Woods, Gregory A. 1994. *Grain growth behavior of the GISP2 ice core from central Greenland.* Penn State, Earth System Science Center, College of Earth & Mineral Sciences.

Zhang, Y, BE Hobbs, and MW Jessell. 1994. "The effect of grain-boundary sliding on fabric development in polycrystalline aggregates." *Journal of Structural Geology* 16 (9): 1315–1325.